1-20-2022

Recent Advances of Wind-Solar Hybrid Renewable Energy Systems for Power Generation: A Review

Pranoy Roy
University of Kentucky, pranoyroy@uky.edu

Jiangbiao He
University of Kentucky, Jiangbiao.He@uky.edu

Tiefu Zhao
University of North Carolina at Charlotte

Yash Veer Singh
Eaton Research Lab

Recent Advances of Wind-Solar Hybrid Renewable Energy Systems for Power Generation: A Review

Digital Object Identifier (DOI)
https://doi.org/10.1109/OJIES.2022.3144093

Notes/Citation Information
Published in *IEEE Open Journal of the Industrial Electronics Society*, v. 3.

IEEE Open Journal of the
Industrial Electronics Society

Received 4 December 2021; revised 3 January 2022; accepted 13 January 2022. Date of publication 19 January 2022;
date of current version 2 February 2022. The review of this paper was arranged by Associate Editor Giovanni Spagnuolo.

Digital Object Identifier 10.1109/OJIES.2022.3144093

Recent Advances of Wind-Solar Hybrid Renewable Energy Systems for Power Generation: A Review

PRANOY ROY [1] (Graduate Student Member, IEEE), JIANGBIAO HE [1] (Senior Member, IEEE), TIEFU ZHAO [2] (Senior Member, IEEE), AND YASH VEER SINGH [3] (Member, IEEE)

[1]Department of Electrical and Computer Engineering, University of Kentucky, Lexington, KY 40506 USA
[2]Department of Electrical and Computer Engineering, University of North Carolina at Charlotte, Charlotte, NC 28223 USA
[3]Eaton Research Lab, Southfield, MI 48076 USA

Corresponding author: JiangBiao He (e-mail: Jiangbiao@ieee.org).

This work was supported in part by the University of Kentucky and the L. Stanley Pigman faculty fellowship endowment.

ABSTRACT A hybrid renewable energy source (HRES) consists of two or more renewable energy sources, such as wind turbines and photovoltaic systems, utilized together to provide increased system efficiency and improved stability in energy supply to a certain degree. The objective of this study is to present a comprehensive review of wind-solar HRES from the perspectives of power architectures, mathematical modeling, power electronic converter topologies, and design optimization algorithms. Since the uncertainty of HRES can be reduced further by including an energy storage system, this paper presents several hybrid energy storage system coupling technologies, highlighting their major advantages and disadvantages. Various HRES power converters and control strategies from the state-of-the-art have been discussed. Different types of energy source combinations, modeling, power converter architectures, sizing, and optimization techniques used in the existing HRES are reviewed in this work, which intends to serve as a comprehensive reference for researchers, engineers, and policymakers in this field. This article also discusses the technical challenges associated with HRES as well as the scope of future advances and research on HRES.

INDEX TERMS Hybrid renewable energy sources, hybrid energy storage system, optimization, power converter, photovoltaic power, wind turbine.

I. INTRODUCTION

An urgent need for alternative sources of energy becomes imminent due to the rapid depletion of fossil fuels, which have been extensively utilized to meet the load demand nowadays. The usage of fossil fuel is also responsible for global warming phenomena [1]. Renewable Energy (RE) sources are the best candidate to provide green energy to overcome this global energy issue. Therefore, it is anticipated that the RE sources will play a pivotal role in the future power supply [2]. For instance, from 2017 to 2018, the cumulative global capacity of renewable electricity increased from 2,181 GW to 2,355 GW. In 2018, renewable electricity was 20.5% of cumulative electricity capacity and provided 17.6% of the total annual generation in the United States [3]. The United States' renewables capacity and generation from 2009 to 2018 are illustrated in Fig. 1.

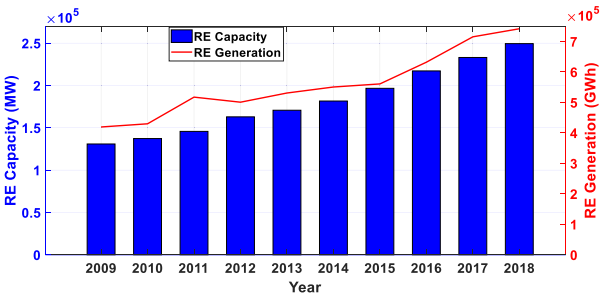

FIGURE 1. U.S. Capacity and Generation: All Renewables (Data obtained from [3]).

As reported in [4], RE was the only energy source which saw increased demand in 2020 despite the pandemic,

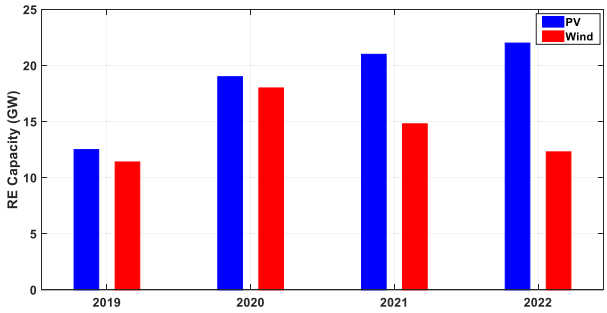

FIGURE 2. Annual PV and wind capacity additions by the USA (Data obtained from [4]).

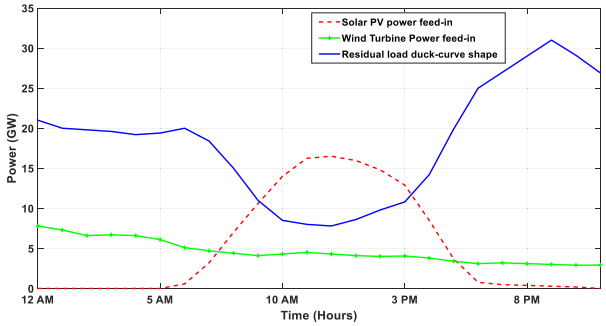

FIGURE 3. Duck curve illustration. Load, solar, and wind profiles for California on March 29, 2013 in a scenario with 11% annual wind and 11% annual solar [9].

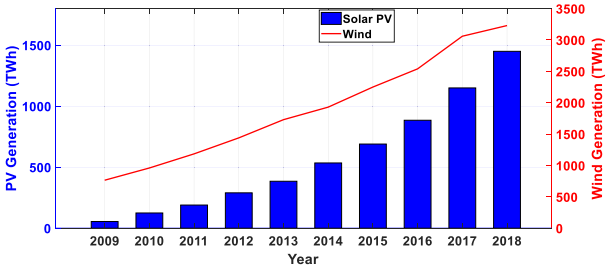

FIGURE 4. Global Electricity Generation by PV and WT (Data obtained from [3]).

while all other fuel consumption declined. Annual renewable capacity additions increased by 45 percent in 2020 to nearly 280 GW, the highest year-on-year increase since 1999. Specifically, solar PV capacity additions are predicted to reach 162 GW by 2022, representing a nearly 50% increase from the pre-pandemic level of 2019. In addition, global wind capacity additions grew by more than 90% in 2020 to 114 GW, a 50% increase from the 2017-2019 average [4]. The annual PV and wind capacity additions by the U.S. are also illustrated in Fig. 2. The U.S. have also provided $280 million in funding for solar power integration and research and $110 million in funding for wind power integration in the fiscal year 2021 budget [5].

According to the U.S. Energy Information Administration (EIA), about 39.7 GW of new electricity generating capacity will come online in 2021, with PV accounting for 39% of the new capacity and wind accounting for 31%. In 2021, 15.4 GW of utility-scale PV capacity is expected to be added to the grid, with four states accounting for more than half of the new utility-scale solar capacity: Texas (28%), Nevada (9%), California (9%), and North Carolina (7%). Furthermore, it is anticipated that approximately 12.2 GW of utility-scale wind capacity is scheduled to come online in 2021, with Texas and Oklahoma states accounting for more than half of the 2021 wind capacity additions, including the 999-MW Traverse wind farm in Oklahoma, which is the largest wind project [6].

It is known that the output of the most renewable energy sources such as photovoltaic (PV) array and wind turbines (WT) substantially depends on ambient environmental conditions. Subsequently, they are producing unstable output characteristics, which is the fundamental disadvantage of renewable energy generations [7]. Thus, various power converters and control strategies are developed for controlling and monitoring active and reactive power, which encounters challenges due to the intermittent nature of renewable energy sources. This kind of power fluctuation poses severe problems for power grid companies such as power quality, load leveling, generation dispatch control, and electric system reliability [8]. The duck curve shown in Fig. 3 can be used to illustrate the considerable challenge of accommodating solar and wind energy, and the potential for overgeneration and curtailment. Fig. 3, modified from [9], illustrates a graph of the total system load of the state of California, the wind and solar PV power feed-in, and the residual load on March 29, 2013. The scenario was considered here with the potential to meet 11% of the annual demand from wind and 11% of the annual demand from solar.

The hybrid utilization of the PV and WT are one of the most promising technologies among renewable energy sources for satisfying the load demand because they have complementary energy generation profiles. Specifically, hybrid renewable energy systems (two or more generation units combined together) can be used to solve such power intermittent issue and enhance power system reliability [10]. Consequently, the penetration of PV and WT energy in power systems has been continuously increasing globally, as is demonstrated in Fig. 4 [3]. Due to the weather and climate patterns, the energy production by Wind-PV resources offset each other on a seasonal or day-to-day basis. For instance, Fig. 5 shows the PV and WT complementary profiles on a day-to-day basis based on actual meteorological data recorded at the National Renewable Energy Laboratory (NREL) on June 10, 2020 [11]. Moreover, the monthly average solar irradiance and wind speed of the U.S. state of Colorado in 2019 are illustrated in Fig. 6 [11]. Note that MATLAB Tools "Basic Fitting" is utilized to increase the resolution of the data in Fig. 5 and Fig. 6.

The wind-solar hybrid renewable energy system (HRES) has the ability to suppress the change of single source output power to some extent. In addition, a properly designed hybrid wind-solar system shows satisfactory performance in

TABLE 1 Recent HRES Projects [14]–[16]

Projects	Specifications	Location
Solar after Sunset	65 MW PV plus 50 MW battery	USA
Solar-storage solicitation	100 MW PV and 100 MW storage	USA
Wheatridge	300 MW of WT, 50 MW of PV and 30 MW of 4-hour duration battery storage	USA
GE Renewables'	2.3 MW WT with 500 kW of PV	USA
NextEra	250 MW WT, 250 MW PV and 200 MW Energy storage	USA
GE Renewables'	1.6 kW WT with 223 kW of PV	India
Le Plana	850 kW WT with 245 kW of PV	Spain
Enel's	497 MW High Lonesome WT project and 450 MW Roadrunner PV project	USA
Fjord	18.9 MW of solar capacity as part of its overall 44.1 MW	Denmark
Vestas	3.3 MW WT and PV hybrid demonstration project	Spain
Flinders Shire	43.2 MW of Vestas WT, 15 MW of PV and a 2 MW, 4 MWh lithium-ion battery	Australia

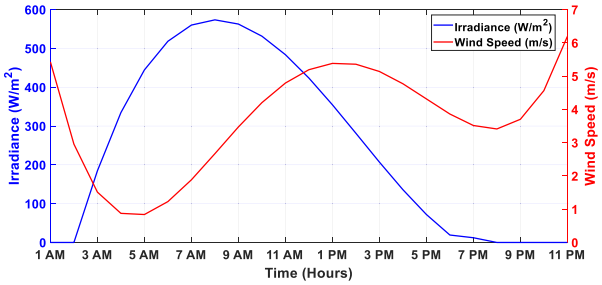

FIGURE 5. PV and WT complementary profiles on day to day basis (Actual meteorological data collected from [11]).

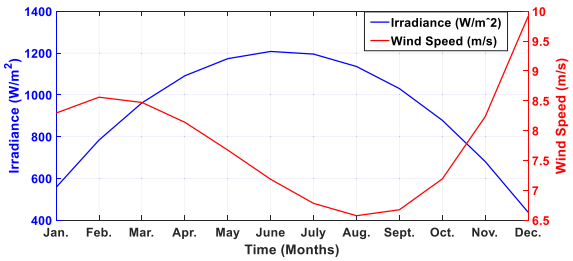

FIGURE 6. PV and WT complementary profiles on seasonal basis (Actual meteorological data collected from [11]).

handling transients compared to a single wind or PV generation for both grid-connected and stand-alone systems [12]. Moreover, the aim is to acquire more stable power output from renewable energy sources, which can be connected with diesel generators, battery banks, ultra-capacitors, or hydrogen production systems. Pumped hydro energy storage (PHES) systems are also employed as an energy storage system (ESS), particularly for large-scale HRES deployment. As the PHES primarily depends on the site specifications, i.e., the height difference, source of water, and the type of land, there is no fixed initial cost or running cost for a PHES, which aids in minimizing the ESS expenditure in the HRES framework [13]. Undoubtedly, the HRES has the ability to improve the reliability and utilization factor of the system. Therefore, the HRES projects at a single location are emerging as a major trend in the global transition to renewable energy. Examples of some practical HRES projects are documented in Table 1 [14]–[16].

The objective of this study is to present a state-of-the-art review that concentrates on analyzing significant research issues about the HRES. The main contribution of this paper can be summarized as follows:

- Different possible combinations and coupling technologies of the HRES have been documented.
- Mathematical modeling of the HRES and characteristics of different energy storage elements have been reported.
- Contemporary power converter configurations for the HRES have been explained.
- Summary of different types of optimization algorithms including the optimization constraints utilized in the HRES has been presented.

The remainder of this paper is structured as follows: the power architectures of the HRES are presented in Section II. The characteristics of different energy storage elements is documented in Section III. The mathematical modeling of the HRES is elaborated in Section IV. The power converter topologies utilized in the HRES are covered in Section V. Commonly used algorithms in the literature for optimizing the HRES are analyzed and summarized in Section VI. The benefits and technical challenges associated with HRES and the scope of future advances and research on HRES are documented in Section VII and Section VIII, respectively. Finally, the conclusions of this review are drawn in Section IX.

II. SYSTEM STRUCTURES OF HRES

A. HYBRID RENEWABLE ENERGY SOURCES

Hybridization techniques can be used to increase the efficiency and reliability of renewable energy sources [17]. Fig. 7 shows different possible combinations of the HRES.

1) HYBRID WIND-SOLAR ENERGY SYSTEM

The hybrid wind-solar energy system incorporates wind and solar energy technologies to produce electrical energy. Due to the complementary profile of wind and solar energy, the hybrid system offers several advantages over the solar or wind energy technology operates alone. It is also noticeable that the peak operating time for wind and solar systems occurs at different times of the day and the year. Therefore, the hybrid wind-solar energy system has the capability to produce more power than the wind or solar energy system operates individually [18].

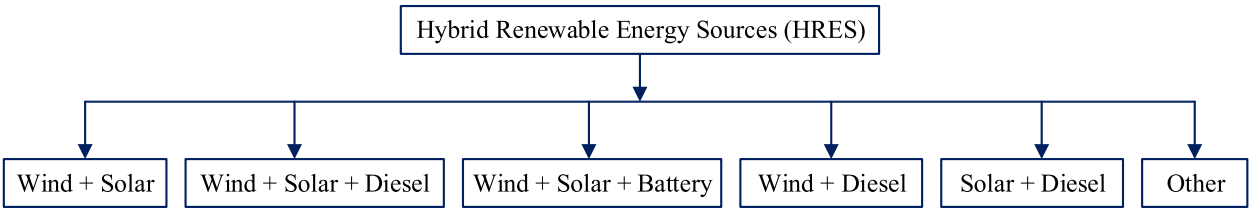

FIGURE 7. **Classification of different types of HRES.**

2) HYBRID WIND-SOLAR-DIESEL ENERGY SYSTEM

The hybrid wind-solar-diesel energy system is an attractive option, especially when a system is not directly connected to electrical distribution or power grid. The diesel generating system, which is powered with non-conventional fuels, is employed as a backup electricity supply source. Basically, a diesel generating system is deployed to ensure the continuity of the electricity supply in the HRES scheme. By adding an engine generator in the HRES framework, the system becomes more complicated. However, modern controllers have the capability to operate these systems automatically. Moreover, the engine generator helps to reduce the size of the power electronic converter needed for the system [19].

3) HYBRID WIND-SOLAR-BATTERY ENERGY SYSTEM

There are several disadvantages, i.e., expensive, bulky, non-environmentally friendly, incorporating a diesel engine in the HRES framework. A battery energy system can be utilized instead of using a diesel generator as a backup emergency option. When the power generated by the renewables is higher than the energy demand, the excess energy can be stored in the battery. Subsequently, it helps to reduce the hybrid system expenditure.

4) HYBRID WIND-DIESEL ENERGY SYSTEM

The hybrid wind-diesel energy system is an exciting alternative to meet the load demand, especially for remote locations. When the wind conditions are satisfactory, a wind-diesel hybrid system can provide enough electricity for such places. The amount of wind power is the deciding factor for designing the hybrid wind-diesel energy system. When the wind power production is always less than the load, other power plants constantly remain in line to control grid frequency and voltage.

5) HYBRID SOLAR-DIESEL ENERGY SYSTEM

Since the PV system hardly has any marginal cost, it is treated with priority on the grid. In this scheme, the diesel generating set is responsible for continuously fill the gap between the load and the actual power generated by the solar energy system. As the generation capacity of diesel generators is limited to a specific range and the solar energy is fluctuating, it is always advisable to include the battery storage to optimize solar energy contribution to the generation of the hybrid system.

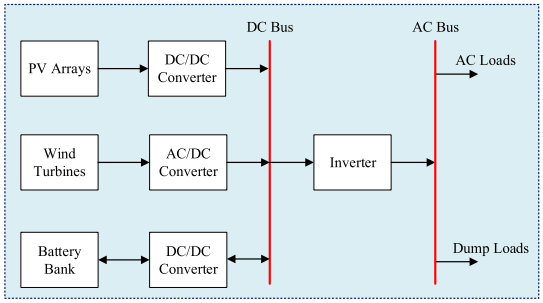

FIGURE 8. **Hybrid PV-Wind-Battery system structure.**

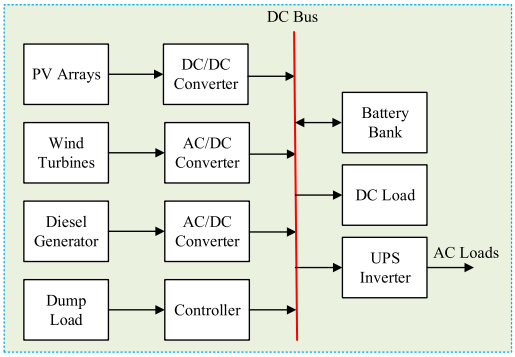

FIGURE 9. **Hybrid PV-Wind-Diesel system structure.**

6) OTHER HYBRID ENERGY SYSTEMS

There are several determining factors, i.e, the cost of hybrid technology, and the availability of natural resources, which the operator needs to consider while designing a hybrid energy system. It is also possible to combine different types of systems and to work as a hybrid system. Wind-hydropower system, solar-hydropower system, solar-wind-geothermal system are some examples of this type of hybrid energy systems [20].

B. SYSTEM ARCHITECTURES OF HRES

A hybrid wind-solar-battery energy storage system is a combination of a wind turbine, a photovoltaic array, and a battery energy storage system. A typical hybrid wind-solar-battery storage system scheme is shown in Fig. 8. In this scheme, the WT, PV arrays, and battery energy storage are connected to a common DC bus through appropriate power converters for the purpose of power conditioning. Another typical hybrid wind-PV-diesel-battery storage system scheme is shown in Fig. 9. According to this scheme, the WT and PV array are

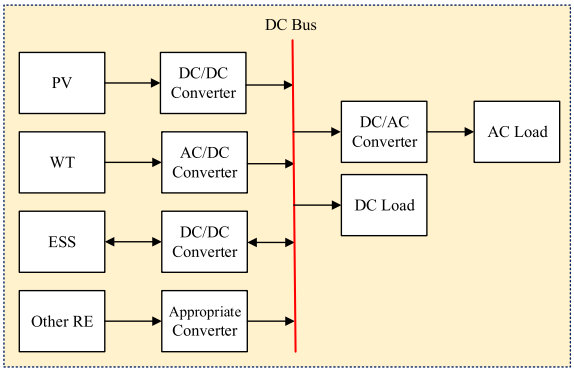

FIGURE 10. DC-Bus connected HRES.

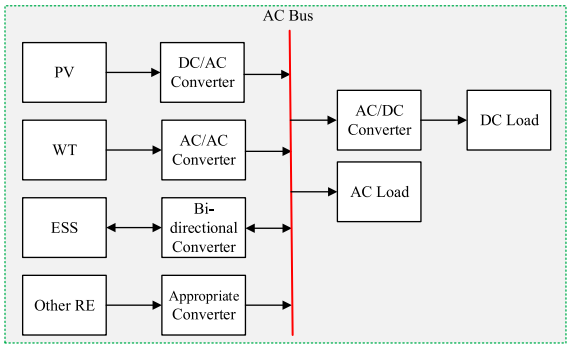

FIGURE 11. AC-Bus connected HRES.

charging the battery while supplying power to the load when the renewable energy is abundant. The purpose of using a dump load is to prevent overcharging of the battery. The controller is responsible for starting the diesel generator, which supplies the load when the state of charge (SOC) of the battery hits the lower limit [21].

C. COUPLING TOPOLOGIES OF HRES

1) DC BUS CONNECTED WIND-SOLAR HRES

Here, the output from the WT is connected to the DC bus through an AC/DC converter, while the output from the PV array is coupled to the DC bus using a DC/DC converter. The energy storage system is tied-up to the DC bus using a bi-directional converter to allow its charging-discharging mechanism. This system framework can serve both AC and DC loads concurrently. A DC/AC converter is required when an AC load needs to be served. In this topology, other sources of RE can also be incorporated using the appropriate power electronic converters. This framework provides several operation advantages, such as simplicity and the elimination of challenges associated with synchronization. The main drawbacks of this architecture are the losses involved with the power conversion systems, particularly the losses associated with converting WT AC power to DC and then back to AC, which is approximately 10% of the WT power [22]. The DC bus connected wind-solar HRES topology is illustrated in Fig. 10.

2) AC BUS CONNECTED WIND-SOLAR HRES

The AC-coupled wind-solar HRES topology is demonstrated in Fig. 11, where the PV coupled to an AC bus using a DC/AC converter and the WT tied-up to the AC bus through an AC/AC converter. The ESS relates to a bi-directional electronic converter. In this scheme, an AC/DC converter is required to feed the DC loads. Other RE sources can be incorporated through the appropriate power converters interface. In this configuration, each of the sources is connected to the AC bus via a separate power converter, allowing them to work even if one of them is disconnected, which can improve the system reliability [22]. Synchronization is the primary impediment of this configuration.

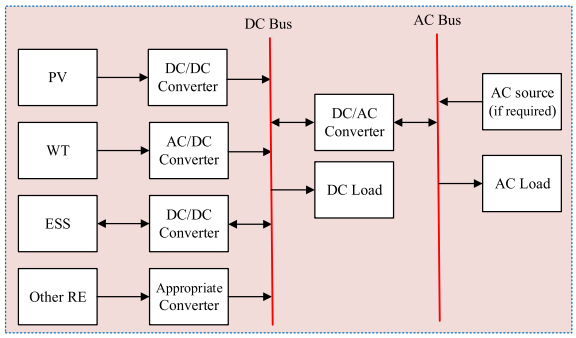

FIGURE 12. Dual-Bus connected HRES (type 1).

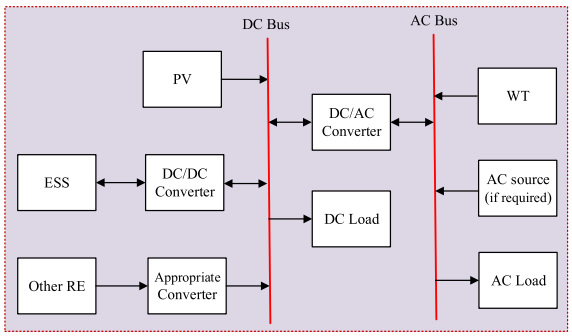

FIGURE 13. Dual-Bus connected HRES (type 2).

3) DUAL BUS CONNECTED WIND-SOLAR HRES

The dual bus-connected wind-solar HRES framework uses both the AC and DC bus. Here, RE sources with AC outputs are directly related to the AC bus, while RE sources with DC outputs are directly coupled to the DC bus. Therefore, the dual-bus connected wind-solar HRES improves overall system efficiency by reducing the number of converters and limiting power losses due to conversion [23]. This configuration is the most widely adopted due to its flexibility to combine energy sources and load irrespective of features [24]. Fig. 12 and Fig. 13 illustrate the dual bus-connected wind-solar configurations.

TABLE 2 **Battery and SC Performance Comparison**

Properties	Battery	SC
Specific energy density (Wh/kg)	10-100	1-10
Specific power density (W/kg)	<1000	<10,000
Energy density (Wh/L)	50-80	2-10
Power density (W/L)	10-400	> 100,000
Power ratings (MW)	0-20	0-0.03
Power capital cost ($/kW)	300-600	100-300
Energy capital cost ($/kWh)	200-400	300-2000
Capital cost ($/kWh-per cycle)	0.2-1	0.02-0.2
Cycle life	1000	>500,000
Charge/discharge efficiency (%)	70-80	85-98
Fast charge time	1-5 hr	0.3-30 sec
Discharge time	0.3-3 hr	0.3-30 sec
Self-discharge rate (% per day)	0.1-0.3	20-40
Operation range temperature ($^{\circ}C$)	-5 to 40	-40 to 75

III. ENERGY STORAGE SYSTEM

By incorporating the ESS in the wind-solar HRES architectures, the uncertainty of renewable resources can also be diminished considerably. In particular, the ESS helps to provide ancillary services; peak regulation, voltage fluctuation and flicker mitigation, harmonic reduction, frequency stability, load leveling, and transient stability. Batteries and Supercapacitors (SC) are the most frequently utilized components among the several types of the ESS in the market. Different types of rechargeable batteries have been found in the market, such as lead-acid, nickel-cadmium, lithium-ion, and lithium-polymer. The design of the battery depends on some system requirements such as (a) voltage and current, (b) charging-discharging rates and duration, (c) operating temperature during charging and discharging, (d) lifetime in terms of the number of charging and discharging cycles, and (e) cost, size, and weight constraints [25].

Examples of practical utility-scale ESS include the 5 MW, 1.25 MWh Li-ion battery installed in the Pacific Northwest smart grid; the 32 MW Li-ion battery installed in a 98 MW wind farm by AES in Elkins, West Virginia; the 8 MW, and the 32 MWh Li-ion battery installed in Tehachapi energy storage project in California [26], [27]. Table 2 shows the relative properties of the lead-acid battery and SC [28]–[30]. The conventional capacitor also exhibits similar characteristics to the SC except that its size is much larger and its cycle life is only half that of the SC [28].

From Table 2, it is noticeable that the battery has the high energy density property, but the low power ramp rate that means the charging-discharging rates of the battery are slow to meet the peak/pulse load demand. On the other hand, the SC has a high power ramp rate, but low energy density property. As a consequence, the SC cannot support the load demand for a long duration. It is evident that none of these two ESS has both the properties of high power density and high energy density. Thus, when only one type of ESS is used to meet both the power and energy capacity requirements, there is a possibility to incur high installation costs. A hybrid energy storage system (HESS) consisting of a battery and SC can be leveraged to develop a more economical energy storage system, where the SC also helps to mitigate the high frequency

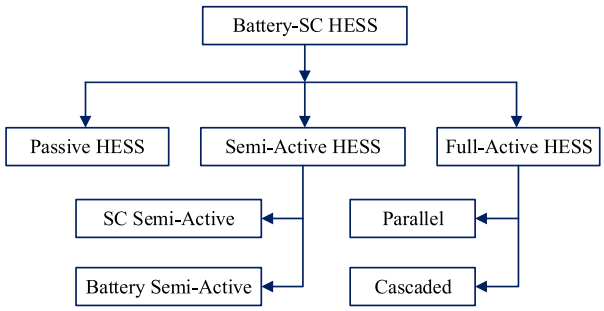

FIGURE 14. **Classification of the battery-supercapacitor HESS topologies.**

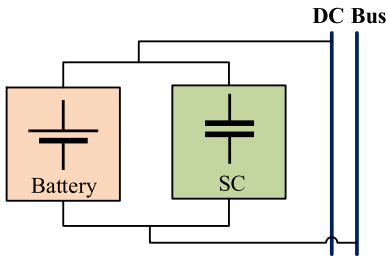

FIGURE 15. **Passive HESS topology.**

power components passing through the battery, which is beneficial for extending the battery lifetime [31].

A. HESS TOPOLOGIES

The HESS can be coupled to either a common DC or AC bus. In general, the HESS can be categorized based on their connection topology as illustrated in Fig. 14 [32], [33].

1) PASSIVE HESS

In the passive HESS framework, the battery and SC are directly connected to the DC bus, as shown in Fig. 15. They share the identical terminal voltage that depends on the SOC and charge-discharge characteristic of the battery. The passive HESS can effectively suppress transient current under pulse load conditions, diminish internal losses, and enhance the peak power. However, as the voltage deviation of the battery terminal is small, the SC can not be operated at its full SOC range, which yields poor volumetric efficiency [34], [35].

2) SEMI-ACTIVE HESS

The power electronic converters can be connected between the ESS and DC bus, which results in the power flow of the ESS to be actively controlled [36]. Either the battery or SC is actively controlled in semi-active HESS topology. A semi-active HESS configuration is illustrated in Fig. 16 (left), where only the SC is interfaced with the DC bus using a bidirectional DC-DC converter that isolates the SC from the DC bus and battery terminal [37]. Here, the SC can be operated within a wider range of voltages that improves its volumetric efficiency significantly. However, the battery is exposed to fluctuating high current in this setting that has an adverse impact on the battery's service life [38].

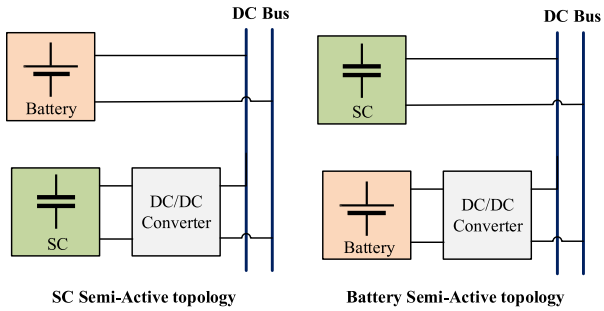

FIGURE 16. Semi-active HESS topology.

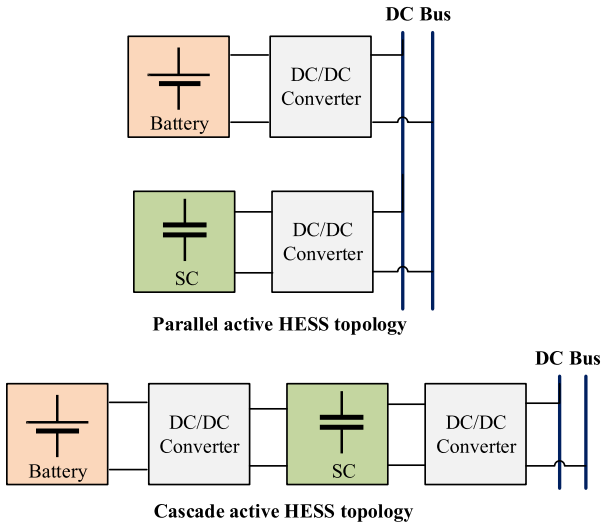

FIGURE 17. Active HESS topology.

The other semi-active HESS framework is demonstrated in Fig. 16 (right). Here, the battery is isolated by a power converter, and the SC is directly connected to the DC bus [39], [40]. In this scheme, the battery's current can be regulated at a moderately reasonable manner in any event of the variation in the power demand. The battery terminal voltage is not necessary to meet the DC bus voltage, which allows the adjustable and economical sizing of the battery bank [41]. However, the linear charge-discharge characteristic of the SC induces substantial fluctuation in the DC bus, which may deteriorate system stability and power quality. The capacity of the SC needs to be comparatively large to maintain a stable DC bus voltage, which leads to an increase in the energy storage expenditure.

3) FULL ACTIVE HESS

The power flow of the battery and SC are both actively controlled through the bidirectional power converters in fully active HESS architecture, which results in enhancing the overall system flexibility and cycle life. Two of the most common full active HESS topologies—(i) parallel active HESS, and (ii) cascaded active HESS—are illustrated in Fig. 17.

Each of the ESS is connected to the DC bus via a bidirectional power converter in parallel active HESS framework [30]. Here, the battery lifetime and DC bus stability can be enhanced through a meticulously designed control strategy [42]. For instance, the frequency management technique can be deployed to increase the longevity of the batteries through comprehensively utilizing the high power density property of SC and the high energy density property of batteries. Besides, the decoupling of battery and SC facilitates both types of the ESS to operate at a comprehensive range of SOC that can make the system more efficient.

In the cascaded framework, two bidirectional power converters are cascaded to seclude the battery and SC from the DC bus [43]. The power converter that separates the battery is typically current-controlled to provide a smooth power transfer with the battery. This mechanism helps the battery to avoid the rapid charging-discharging process corresponding to increase in the battery service life. The power converter that segregates the SC from the DC bus is usually voltage-controlled to inhibit the DC bus voltage while absorbing the fast-changing power exchanges [44]. It is expected that a substantial voltage swing between the SC and DC bus due to the SC has a wide operating voltage. As a consequence, the power losses in the power converter considerably increase as it is challenging to regulate efficiency over a wide range of operating voltages.

The overall efficiency of the HESS substantially decreases as the number of DC/DC converter increases. Moreover, the performance of fully active HESS architecture is heavily dependent on the reliability of the power converters and their control system.

IV. MODELING OF HRES

According to the different parameters and constraints, modeling is the first step in designing a renewable energy system. In this section, the authors attempt to document the PV, WT, Battery, and SC mathematical modelings, which will be useful to researchers to understand the characteristics of these components.

A. MODELING OF PV SYSTEM

In the literature, there are many mathematical models developed to describe the behavior of the PV [45], [46]. A PV cell is a nonlinear device that can be represented as a current source model. The V-I characteristic equation of a PV cell is shown in (1) and (2).

$$I = I_{sc} - I_d \tag{1}$$

$$I = I_{sc} - I_{os}\left(e^{\frac{q.(V+I.R_S)}{n.K.T}} - 1\right) \tag{2}$$

where I_{sc} is the light generated current, I_{os} is the diode reverse saturation current, q is the electronic charge, k is the Boltzmann constant, T is the temperature, V is the terminal voltage of the module, and R_s is the series resistance.

The output of the PV array depends on two weather conditions: solar irradiation (W/m^2) and solar cell temperature (°C).

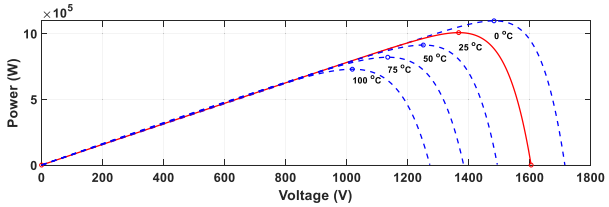

FIGURE 18. Power-Voltage characteristics of PV array at various temperatures.

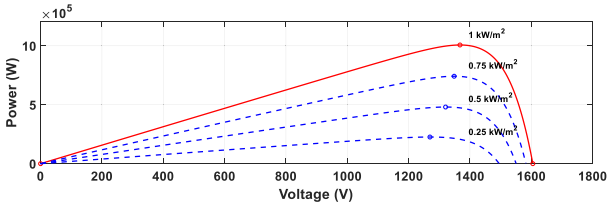

FIGURE 19. Power-Voltage characteristics of PV array at various irradiance.

The PV array module in Matlab/Simulink provides power-voltage characteristic curves based on user-input parameters, such as solar cell type, the number of cells in parallel, and the number of cells in series, under various weather conditions. The power-voltage characteristic curves for 1 MW PV array are shown in Fig. 18 and Fig. 19. At maximum power point (MPP) operation, the PV arrays' output power is marked as a circle of their respective curves. The maximum power point tracking (MPPT) technique is generally employed to extract the maximum power from the PV array. The incremental conductance (IC), perturb & observe (P&O), short circuit current (SCC), and open circuit voltage (OCV) are commonly MPPT approaches utilized in the PV system [47]. In general especially for residential PV framework, the PV array provides power to the unidirectional boost converter, and an MPPT is utilized to control the duty ratio of the power converter to extract maximum power from the PV array.

The authors in [48] described a simplified technique to calculate the PV output power, which can be expressed as:

$$G(t, \theta_{pv}) = G_v(t) \times \cos(\theta_{pv}) + G_H(t) \times \sin(\theta_{pv}) \tag{3}$$

$$P_{pv} = \frac{G}{1000} \times P_{pv,rated} \times \eta_{MPPT} \tag{4}$$

where G is perpendicular radiation at the arrays' surface (W/m^2). $P_{pv,rated}$ is rated power of each PV array at G equal to 1000 (W/m^2) and η_{MPPT} is the efficiency of PV's power converter and MPPT.

Another simple model is contemplated in [49] to predict the PV output power as a linear function of effective irradiance, as shown in (5). This model has the advantage of being parameterized from the PV panel datasheet and being simple to use, however it is not precise and does not account for environmental factors such as wind speed and solar cell temperature on PV performance.

$$P_{mp,array}(\rho_e) = N_s \times N_p \times \left(\frac{\rho_e}{\rho_s} P_{mp,s}\right) \tag{5}$$

where $P_{mp,array}$ is the PV power at the maximum point for PV array, N_s and N_p are the number of panels and number of subarray, respectively, ρ_e is the effective solar irradiance, ρ_s is the solar irradiance under STC (1000 W/m^2), and $P_{mp,s}$ is the PV power at the maximum point for PV module.

Normally, the PV cell temperature is much higher than the ambient temperature, and it can decrease the PV output power as well as its capacity factor. An effective approach for estimating the PV cell temperature is formulated in [50]:

$$(T_m^{\circ}C) = a \times T_a + b \times I_r - c \times V_w + d \tag{6}$$

where, a, b, c, and d are system-specific regression coefficients, T_a refers to the ambient temperature given in (°C), I_r refers to the solar irradiation given in (W/m^2), and V_w refers to the wind speed given in m/s.

The curve fitting tool is utilized to calculate the regression coefficients a, b, c, and d. Thus, the formula for prediction of the PV cell temperature can be expressed as:

$$(T_m^{\circ}C) = 0.943 \times T_a + 0.0195 \times I_r - 1.528 \times V_w + 0.3529 \tag{7}$$

Sandia National Laboratory proposed another PV cell temperature estimation model known as the Sandia Model [51]. The PV model estimates the impact of PV cell temperature on PV performance using data from ambient temperature and wind speed. The public parameter databases as well as additional information about this model are available in [52]. The Sandia Model is highly accurate and can be expressed as:

$$I_{mp}(\rho_e, T_c) = I_{mp,ref}\left(C_0 \times \rho_e + C_1 \times \rho_e^2\right)[1 + \alpha(T_c - T_s)] \tag{8}$$

$$V_{mp}(\rho_e, T_c) = V_{mp,ref} + C_2 n_s \delta(Tc) \ln(p_e) + C_3 n_s \left[\delta T_c \ln(p_e)\right] + \beta_{mp}(T_c - T_s) \tag{9}$$

$$P_{mp,array} = N_s \times N_p \times V_{mp} \times mp \tag{10}$$

B. MODELING OF WT SYSTEM

There are several existing models in the literature review to estimate the wind turbine power including linear, cubic, quadratic, Weibull parameters, and so on [53]–[55]. Generally, the output power of the wind turbine is a function of aerodynamic power efficiency, wind speed distribution of the selected sites, mechanical transmission and electrical energy conversion efficiency, and the hub height of the wind tower.

Sami *et al.* described a wind turbine model in [56] to calculate the WT power generation output.

$$P_W = \begin{cases} P_r\left(\frac{V^2 - V_c^2}{V_r^2 - V_c^2}\right), & V_c \le V < V_r \\ P_r, & V_r \le V < V_f \\ 0, & V \ge V_f \end{cases} \tag{11}$$

where P_W is the output power of the wind generator, P_r is the rated power of the wind generator, V_c is the cut in speed of the WT, V_r is the rated speed of the WT, and V_f is the cut-out speed at which the WT stops rotating.

When the meteorological data recorded is found at a different height from the WT height, (12) is utilized to calculate the wind speed:

$$V_h = V_{ref}\left(\frac{H}{H_{ref}}\right)^{\alpha} \tag{12}$$

where V_h is the wind speed at turbine height (H), V_{ref} is the wind speed recorded by a meteorological station at height (H_{ref}) and α is the surface roughness factor which is around 1/7 in an open space surface [57].

The permanent magnet synchronous generator (PMSG) coupled wind turbine system (WES) has been reported in the studies [58], [59]. The PMSG based on WES can associate with the WT without utilizing a gearbox. The energy conversion in PMSG based on WES takes place through two stages. First, the kinetic energy is captured by the WT blades as mechanical energy. Second, the mechanical energy is transferred through the shaft to PMSG, which converts the mechanical energy to electrical energy. The mechanical output power of a PMSG wind turbine can be expressed as:

$$P_m = \frac{1}{2}\rho A v_w^3 C_p(\lambda, \beta) \tag{13}$$

where P_m is mechanical output power of the turbine (W), ρ is air density (kg/m^3), A is turbine swept area (m^2), v_w is wind speed (m/s), C_p is the performance coefficient of the turbine, λ is tip speed ratio of the rotor blade tip speed to wind speed and β is blade pitch angle (degree).

The mechanical output power P_m depends significantly on the turbine performance coefficient C_p. In this study, the following generic $C_p(\lambda, \beta)$ model is employed:

$$C_p(\lambda, \beta) = c_1\left(\frac{c_2}{\lambda_i} - c_3\beta - c_4\right)e^{\left(\frac{-c_5}{\lambda_i}\right)} + c_6\lambda \tag{14}$$

$$\frac{1}{\lambda_i} = \frac{1}{\lambda + 0.08\beta} - \frac{0.035}{\beta^3 + 1} \tag{15}$$

where, $c_1 = 0.5176$, $c_2 = 0.116$, $c_3 = 0.4$, $c_4 = 5$, $c_5 = 21$, and $c_6 = 0.0068$. The consequent C_p-λ curve is illustrated in Fig. 12. The C_p-λ curve shows that the maximum value of C_p is achieved for $\beta = 0$ and $\lambda = 8.1$.

The WT model in MATLAB/Simulink provides the WT power characteristic curve based on user input parameters such as base wind speed, base rotational speed, blade pitch angle (β), and maximum power at base wind speed. The WT power characteristics curve is illustrated in Fig. 20. In this power curve, β is assumed to be zero and wind speed varies from 5 m/s to 11 m/s. The maximum power points for each wind speed are labelled. The generator rotor speed should track the wind speed changes to extract the maximum power from the wind. In general, the back to back power converters are employed to meet the power quality criteria while the WES generated power is transferred to the utility.

C. MAXIMUM POWER POINT TRACKING

The maximum power generated by the PV generators varies with solar irradiance and temperature. Since the PV exhibits non-linear current-voltage and power-voltage characteristics, any alteration in solar insolation and temperature causes a change in terminal voltage, resulting in deviation from maximum power generation. The MPPT is utilized to adjust the solar operating voltage close to the MPP in response to changing atmospheric conditions in order to maximize power harvest from the PV array. As a result, it has become an essential component in evaluating the design performance of PV power systems.

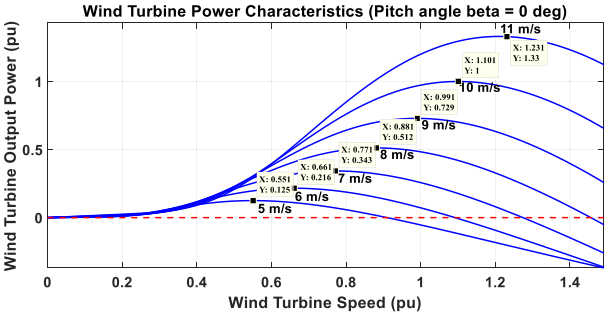

FIGURE 20. WT power characteristics curve.

In the literature, approximately 40 different methods are reported to track the maximum power point. This availability of multiple options as an MPPT makes its unambiguous selection a tougher nut to crack. The authors in [60] contemplated a summary of 31 different kinds of MPPT techniques, and a comparative comparison was documented among them based on 12 factors: category, dependency of PV array, implementation methodology, sensor required, stages of energy conversion, partial shading enabled, grid integration, analog or digital, tracking efficiency, tracking speed, cost, and product availability on the market. Furthermore, the authors also classified MPPT techniques into three categories based on control strategy, such as indirect control methods (mathematical methods based on empirical data), direct control methods (modulation-based control strategies), and soft computing technique-based methods (genetic algorithm, particle swarm optimization, and artificial neural network).

A comprehensive review of MPPT techniques for PV systems under normal and partial shading conditions (PSC) was conducted in [61]. The selected MPPT strategies are classified further into three categories: artificial intelligence, hybrid, and other MPPT methods. It is reported that researchers have concentrated more on PSC in recent years in order to increase the power output and efficiency of PV systems. Another comparative study, which included the detailed classification and description of MPPT strategies for PV systems available until 2012, is summarized in [62]. The available MPPT strategies are classified based on the number of control variables involved, types of control strategies, circuitry, and cost of applications, which is useful for selecting an MPPT approach for a certain application.

In [63], the existing MPPT techniques are divided into two main categories: classical MPPT and modern MPPT, and the tactics of each category are briefly discussed. The

modern MPPT category includes fuzzy logic, artificial neural network, and metaheuristic-based MPPT techniques, whereas the classical MPPT category includes perturb and observe, hill climbing, fractional open circuit voltage, and fractional short circuit current. The performance of each MPPT strategy is compared in both uniform and PSC insolation, and the mataheuristic-based MPPT technique outperformed the other MPPT approaches investigated in extracting the maximum power from the PV array due to several advantages, including system independence, effective performance in PSC, and the absence of oscillations around the maximum power point.

The authors in [64] contemplated another survey on MPPT approaches by categorizing several existing MPPT techniques into three broad categories: offline, online, and hybrid methods. Offline MPPT techniques include open circuit voltage (OCV), short circuit current (SCC), and artificial intelligence (AI) based MPPT methods, which are referred to as model-based approaches because the physical values of the PV panel are utilized to generate control signals. On the other hand, the online category encompassed perturbation and observation (P&O), extremum-seeking control (ESC), and incremental conductance (IncCond) MPPT techniques, which are referred to as model-free methods where the relationship between the open circuit voltage and the maximum power point voltage is used to generate the control signals. Hybrid methods are a combination of online and offline approaches. The control signal associated with the hybrid method consists of two parts, where the first part is generated based on model-based techniques and the latter part is generated based on model-free approaches. The MPPT strategies are compared in terms of the dynamic response of the PV system, achievable efficiency, and implementation considerations, and hybrid methods outperformed model-based and model-free methods in extracting the maximum PV power.

Due to the variable nature of the wind, it is desirable in the wind energy conversion system to determine the optimal generator speed that assures maximum energy production. The MPPT approach is used to optimize the generator speed in relation to the wind velocity intercepted by the WT, ensuring the maximum energy is harvested from the available wind at any instance. Many MPPT strategies have been reported in the literature, and these methods differ in terms of technique employed, complexity, number of sensors required, convergence speed, memory requirement, range of effectiveness, and so on. These MPPT techniques can be primarily classified as tip-speed ratio control (TSR), power-signal feedback (PSF), and hill climb search (HCS) based [65]. However, so many variations have been proposed over the last 30 years that it has become difficult to decide which strategy, newly proposed or existing, is best suited for a particular wind system.

The TSR control method regulates the rotational speed of a wind turbine generator to maintain an appropriate TSR, and this method requires the estimation of both wind speed and turbine speed, which is typically derived from turbine-generator characteristics and varies from system to system. Likewise, the PSF technique requires the knowledge of a wind turbine's maximum power curve to estimate the optimum turbine speed for a specific wind velocity to harvest the maximum available power from a WT [66]. Because both TSR and PSF control techniques involve substantial turbine knowledge as well as measurements of generator and wind speed, the practical implementation of the algorithm becomes highly complicated as the number of sensors and control complexity increase significantly. The HCS-based MPPT approaches are proposed to tackle these challenges, in which the algorithm continuously searches for a turbine's peak output power by altering the generator speed and adjusting the power direction. However, due to the constraints of deteriorated power quality, as power ripple constantly persists and the tracking speed is typically slow, its utilization is confined to small-scale wind turbine systems [67]. While each of these three strategies has advantages and disadvantages, a variety of versions of these methods have been presented over the years, each employing a different methodology to handle these concerns. The most significant aspects to consider while selecting a specific MPPT strategy are contemplated in Table 3 [68], [69].

D. DEGRADATION MODEL OF ESS

Addoweesh *et al.* described a simple battery model in [70], where the SOC of the battery is calculated by a comprehensive analysis of the battery's charging-discharging modes, load profile, and output energy of the renewable energy sources.

$$SOC(t) = SOC(t-1)(1-\sigma) + \left(E_{GA}(t) - \frac{E_L(t)}{\eta_{inv}}\right)\eta_{bat} \tag{16}$$

where $SOC(t)$ and $SOC(t-1)$ are the SOC of the battery bank at time t and t-1; σ is hourly self-discharging rate; $E_{GA}(t)$ is the total energy generated; $E_L(t)$ is the load demand; η_{inv} and η_{bat} are the efficiencies of inverter and battery.

1) LI-ION BATTERY DEGRADATION MODEL

To consider cycling and calendar aging for battery usage, a degradation model proposed in [71] is documented in this study. The expected lifetime of the battery decreases due to its degradation properties over the period, which can be expressed as:

$$\frac{1}{T_{life}} = \left[\sum_{i=1}^{N} \frac{DOD_i^2}{2\,N_{cycles}^{ref}} + \frac{T}{T_{calendar}^{ref}}\right] \times e^{\left(\frac{\theta_c - \theta_c^{ref}}{\theta_0}\right)} \tag{17}$$

where T_{life} is the battery's service life, in years, decreases due to its degradation properties, N is the total number of half-cycles over the simulation period T, i is the index of the half-cycle, DOD_i is the DOD during the half-cycle i, θ_c is the case temperature, and θ_0 is the ambient temperature. $T_{calendar}^{ref}$ is the lifetime, in years, for a case temperature of θ_c^{ref}. A rainflow-counting algorithm is generally employed to determine all half-cycles. The parameters N_{cycles}^{ref}, $T_{calendar}^{ref}$, θ_0 and θ_c^{ref} are presented in Table 4 [71].

TABLE 3 Comparison of Characteristics of Various MPPT Techniques [68], [69]

Technique	Complexity	Convergence speed	Prior knowledge	Memory requirement	Wind speed measurement	Performance under varying wind conditions
TSR control	Simple	Fast	No	No	Yes	Very good
Optimal torque control	Simple	Fast	Yes	No	No	Very good
PSF control	Simple	Fast	Yes	Yes	Yes	Good
HCS control	Simple	Depends	No	No	No	Good
Adaptive HCS control	High	Medium	No	No	No	Good
Flux estimated	High	Slow	No	Depends	No	Moderate
Pitch control	Medium	Slow	Yes	No	Yes	Poor
Neural network	High	Fast	Yes	Yes	Depends	Very good
Fuzzy logic	High	Fast	Yes	Yes	Depends	Very good
Lookup table	Simple	Fast	Yes	Yes	Yes	Very good
Theoretical based	Simple	Fast	No	No	No	Poor
Other methods	High	Medium	Yes	Yes	No	Good

TABLE 4 Parameters of the Li-Ion Battery Aging Model

N_{cycles}^{ref}	16,000
$T_{calendar}^{ref}$	25 years
θ_c^{ref}	25° C
θ_0	22 K

In [72], another degradation model is reported for battery usage where the calendar aging cost of the battery ($C_{Bat,calendar}$) considering of its depth of discharge (DOD) usage and the initial cost is calculated as follows:

$$C_{Bat,calendar} = \frac{C_B}{C_{B,n} \times 2 \times DOD \times E_B \times m^2} \tag{18}$$

where $C_{B,n}$ is the life cycle of the battery provided by the manufacturers, E_B is the battery capacity (kWh), C_B is the battery cost ($/kWh), and m is the efficiency of the battery that was assumed 92% for a Li-ion battery.

2) SC AGING MODEL

An aging model for the SC is contemplated in this study that considers both calendar aging and cycling aging [73]. The expected lifetime of the SC ($T_{SC,life}$) can be expressed as:

$$\frac{1}{T_{SC,life}} = \frac{1}{T_{life}^{ref}} \times \exp\left(\ln(2)\frac{\theta_c - \theta_c^{ref}}{\theta_0}\right) \times \left[\exp\left(\ln(2)\frac{V - V^{ref}}{V_0}\right) + K\right] \times \exp\left(K_{RMS}\frac{I_{RMS}}{C_0}\right) \tag{19}$$

where $T_{SC,life}$ is the SC lifetime in hours, θ_c is the case temperature and V is the voltage across the component. V_0 and θ_0 are the respective decreases in voltage and temperature necessary to double the SC service life. T_{life}^{ref} is the lifetime, in hours, for a case temperature of θ_c^{ref} with a voltage of V^{ref}. K is a dimensionless constant that replaces the voltage term whenever the voltage is low. C_o is the initial value of the SC capacitance, and K_{RMS} is an accelerator factor. I_{RMS} is the RMS current flowing through the component. The parameters of the SC aging model are given in Table 5 [73].

TABLE 5 Parameters of the SC Aging Model

θ_0	7.7 K
V_0	89 mV
K	29×10^{-3}
T_{life}^{ref}	1470 h
V^{ref}	2.7 V
θ_c^{ref}	65° C
K_{RMS}	68 s.V^{-1}

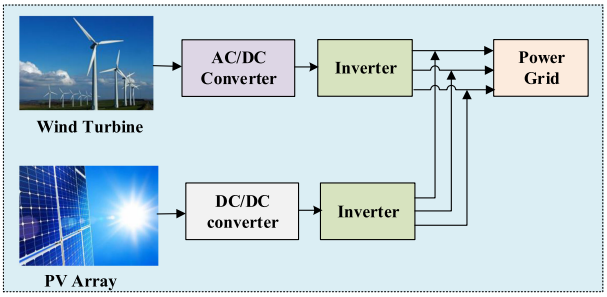

FIGURE 21. AC shunt coupled HRES.

V. POWER CONVERTER CONFIGURATIONS FOR HRES

Various power converters have been utilized in the HRES to extract the maximum power from the source, interface the different energy sources, and regulate the power quality at the load side. In general, the back-to-back AC-DC-AC power converter is employed to integrate the WT into the utility, and the unidirectional boost or buck-boost converter along with inverter is deployed to integrate the PV into the grid. In a hybrid PV-Wind configuration, the total cost with the semiconductor switches can be saved by up to 25% through the development of multi-port power converters where one single converter can interface several energy resources [74]. In general, the power converter configurations employed in the HRES can be classified into three categories, as follows: (i) AC shunt coupled HRES, (ii) DC shunt coupled HRES, and (iii) Multi-input coupled HRES.

A. AC SHUNT COUPLED HRES

The AC shunt coupled grid-connected HRES is illustrated in Fig. 21, where two separated inverters are deployed for the

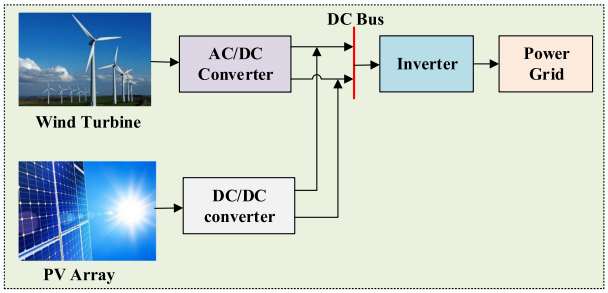

FIGURE 22. DC shunt coupled HRES.

HRES grid integration. In this framework, one DC-DC converter (e.g., buck-boost converters) embedded with maximum power point tracking (MPPT) algorithms is connected with the PV system, and one AC-DC active rectifier is generally configured to interface the WT generator. Individual inverters are employed to convert the PV and WT system's DC power into the AC, and eventually incorporated at the AC bus and fed to the utility grid. The AC shunt coupled solution is straightforward and simple in controls, but one potential drawback is that it requires the synchronization of two energy sources.

B. DC SHUNT COUPLED HRES

In DC shunt coupled HRES architecture, one single common inverter is utilized for integrating the hybrid PV-Wind system into the utility grid, which is shown in Fig. 22. Here, the power converters are utilized for converting the PV and wind power into DC power. One common central inverter is employed to convert and manage the DC power into AC power and integrated for the utility grid. The inverter serves as an interface between the source and utility grid in this framework. This DC coupled solution yields higher efficiency and higher power density in many scenarios due to lower number of cascaded converters. However, one likely shortcoming is that, when the common inverter fails, the whole system will be malfunctioned.

C. MULTI-INPUT COUPLED HRES

The AC or DC shunt coupled HRES requires multiple converters and the associated controllers as well as communication techniques between individual converters. As a result, the cost associated with the HRES increased substantially. To address this challenge, multi-input converter (MIC) have been proposed and developed, which is capable of interfacing different renewable energy sources and energy storage systems in one single power stage to achieve individual and simultaneous power transfer to the utility grid. The MIC offers several advantages, i.e., simple circuit topology with a reduced number of semiconductor switches, centralized control, and low manufacturing expense and size [75]. The MIC can be further divided into three categories, namely, (i) Non-isolated MIC, (ii) Isolated MIC, and (iii) Semi-isolated MIC.

Fig. 23 illustrates the non-isolated MIC, which is comprised of a buck and buck-boost fused multi-input DC-DC converter

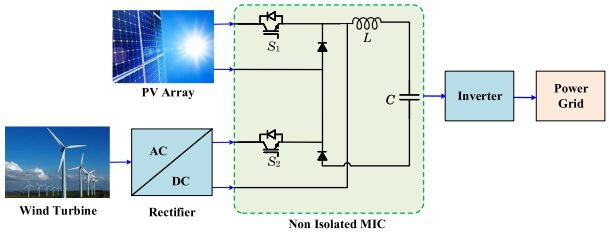

FIGURE 23. Non-isolated MIC coupled HRES.

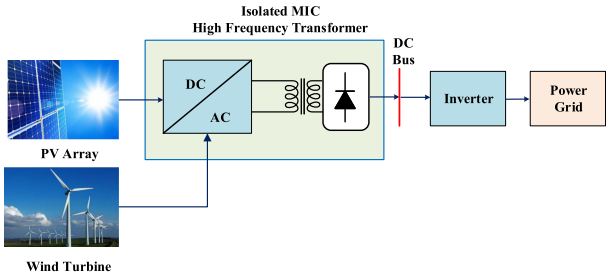

FIGURE 24. Isolated MIC coupled HRES.

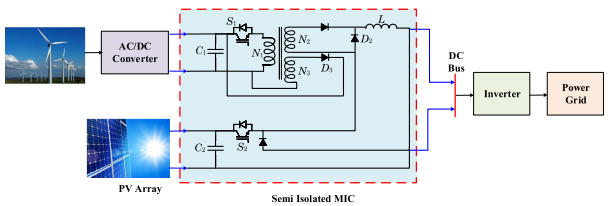

FIGURE 25. Semi-isolated MIC coupled HRES.

and an inverter [76]. In this topology, the rectified WT output and PV output are fed as inputs to the MIC. The maximum power from renewable energy sources can be extracted individually and simultaneously by applying the appropriate switching scheme with a suitable MPPT algorithm in this framework. Then, the inverter with an appropriate control and modulation scheme is employed for converting the regulated DC power into AC power to meet the grid specifications. In this solution, galvanic isolation is unavailable between the source and load, which may induce significant common-mode current and EMI issues.

The isolated MIC is illustrated in Fig. 24, which consists of a multi-input isolated DC-DC converter and an inverter. The high-frequency transformer is utilized in the isolated MIC configuration to provide the galvanic isolation between the source and load. It can extract the maximum power from both energy sources individually and simultaneously, and meanwhile can regulate the low-level DC voltage. The required sinusoidal AC power can be obtained by utilizing the inverter with appropriate control and modulation strategies in this framework. The size of the high-frequency transformer can be reduced by leveraging the emerging wide bandgap switches and operating at high switching frequency (e.g., tens of kHz).

TABLE 6 Types of Power Converter Configurations Implemented in Wind-Solar HRES

Ref.	System Topology	Converter Configuration	Highlights
[77]	PV-WT-BESS	AC shunt coupled	Improve smoothing performance of the HRES; Novel SOC control strategy of the BESS; Effectively regulate the HRES power output levels.
[78]	PV-Wind-ESS	AC shunt coupled	Evaluate the ESS control strategy for HRES during fault-ride condition; Analyze the dynamic performance of superconducting magnetic energy storage system to protect the critical loads.
[79]	PV-WT-BESS	AC shunt coupled	Economic analysis using genetic algorithm; Implement a supervisory controller to manage energy between the HRES units.
[80]	PV-WT-BESS	AC shunt coupled	Flexible power control of each HRES unit; Decentralized power management strategy.
[81]	PV-WT	DC shunt coupled	Extending PI controllers are employed to extract the maximum power from the PV-WT scheme; The total harmonic distortion (THD) is found within a grid compliance standard.
[82]	PV-WT-BESS	DC shunt coupled	Investigate power-control techniques of a HRES with versatile power transfer; A supervisory strategy is employed to regulate the power generation of the individual HRES units.
[83]	PV-WT-BESS	DC shunt coupled	Optimal BESS sizing; Cost minimization of the HRES; Improve power quality injected into the grid; Increase power supply reliability.
[84]	PV-WT-BESS	DC shunt coupled	Simple power management technique; Reduce the number of power converter for HRES; Eliminate the need for dump loads; Improve HRES efficiency.
[85]	PV-WT-HESS	DC shunt coupled	Hourly dispatching scheme of the HRES is demonstrated; Optimal scaling of the HESS is investigated; Economic analysis of the ESS is presented.
[74]	PV-WT	Non-isolated MIC	Unique nine-switch front end configuration for connecting HRES units; Reverse-boost mode; Accurate power dispatch.
[86]	PV-WT	Non-isolated MIC	Propose front-end rectifier configuration for hybrid PV-Wind framework; Eliminate the need for input filter; Adaptive MPPT is employed to extract the maximum power from the HRES.
[87]	PV-WT-Fuel cell-BESS	Non-isolated MIC	Improve reliability and dynamic response of the HRES; Proposed strategy works in both transient and steady-state power sharing modes.
[88]	PV-WT-Fuel cell-BESS	Non-isolated MIC	Five port DC-DC converter; Load dynamic regulation; Improve reliability of the HRES.
[89]	PV-WT	Isolated MIC	Simple framework; Energy management; Minimum number of power switches.
[90]	PV-WT-BESS	Isolated MIC	Four port DC-DC converter; Dynamic modeling and closed loop design; Feature low component count and zero-voltage switching operation.
[91]	PV-WT	Semi-isolated MIC	Simplify the power system; Deliver continuous power; Minimize the cost; Overcome high-voltage-transfer-ratio problem.
[92]	PV-WT-BESS	Semi-isolated MIC	Zero-voltage switching is realized for all primary switches; Bidirectional capability; Low component count; Achieved maximum power harvesting for PV and/or WT.
[93]	PV-WT-BESS	Non-isolated MIC	Utilizes only four power switches which are independently controlled with four different duty ratios; Newton-Raphson algorithm based maximum power point tracking strategy is proposed for PMSG variable speed WT generating system.
[94]	PV-WT-BESS	Semi-isolated MIC	Reduced number of power conversion stages; Less component count; Higher efficiency and reliability; Optimal charging of the ESS utilizing multiple sources; Simple control strategy.
[95]	PV-WT	Isolated MIC	Compact structure; Automatic load regulation; Soft switching; Regulates zero-current switched turn-off under a wide load, as well as input voltage variations.

A semi-isolated MIC is shown in Fig. 25. It is comprised of both non-isolated converters for obtaining the maximum power from renewable energy sources and isolated converters for galvanic isolation. The different types of power converter configurations employed in the state-of-the-art wind-solar HRES are summarized in Table 6.

D. INVERTER CONFIGURATIONS FOR HRES

The grid inverters play a critical role in the HRES, not only converting the DC power into AC power to be integrated grid, but also may provide ancillary grid service if needed. Grid inverters can be classified into two broad categories: self-commutated inverter and line-commutated inverter. The turn-on and turn-off characteristics of the switching devices depend on the polarity of the current flow in the line-commutated inverter. However, the self-commutated inverter can be employed with full control of the switching devices.

The commutation process in the line-commutated inverter is initiated by the parameters of the grid, i.e., the reversal of AC voltage polarity and the flow of negative current. In general, the semi-controlled power switching devices, such as thyristors, are utilized in this scheme. Although the turn-on process of the semiconductor power switches can be controlled by the gate terminal of the device, an external circuitry, i.e., anti-parallel diode, is required to control the turn-off operation as well. The schematic diagram for a line-commutated current source inverter (CSI) is shown in Fig. 26 (left) [96].

The self-commutated inverter is the fully controlled power converter, as shown in Fig. 26 (right) [97]. The power switching devices, such as IGBTs or SiC MOSFETs, are utilized in the self-commutated inverter configuration. This framework

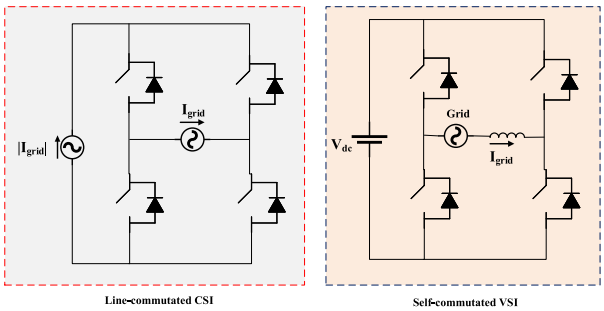

FIGURE 26. Grid-connected inverters.

also provides the facilitates to enable the current transfer from one switching device to another in a controlled manner. The self-commutated inverter can be divided into voltage source inverter and current source inverter.

Based on the existence or absence of the transformer, the inverter configuration can be classified into two categories, i.e., those with transformers and the transformerless ones. When a transformer is embedded in the inverter configuration, it provides galvanic isolation between the HRES and the utility grid. Since the transformers are bulky and costly, the overall expenditure of the HRES will be increased considerably in comparison with the transformerless inverter scheme. In transformerless inverter topology, the inverter output are generally medium-voltage levels, and additional circuitry may be needed to address the problem of DC current injection. Furthermore, as there is no galvanic isolation in the transformerless inverter architecture, it might induce voltage fluctuation, common mode voltage, and leakage current issues between the RE sources and the ground [98].

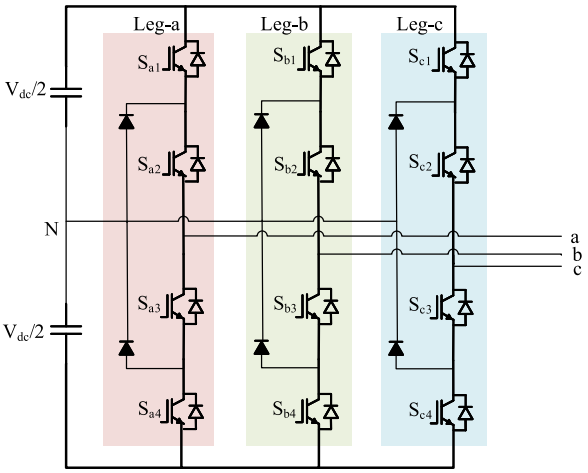

FIGURE 27. Circuit topology of 3-level I-type NPC inverter [111].

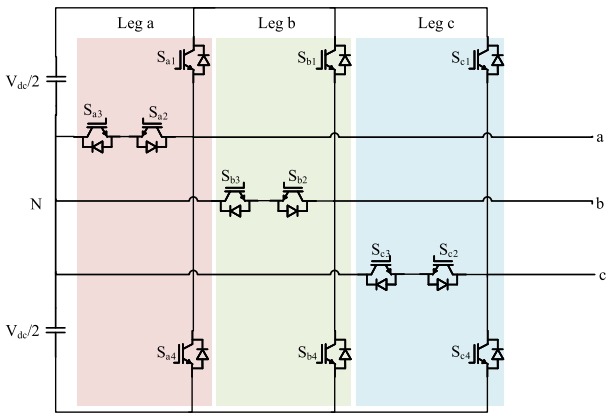

FIGURE 28. Circuit topology of 3-level T-type NPC inverter [111].

1) MULTILEVEL INVERTERS

Multilevel inverters are the power inverters that utilize a large number of semiconductor switches, which can withstand higher DC-link voltage and synthesize staircase quasi-sinusoidal waveforms. Thus, the output line voltages possess much lower THD, lower dv/dt, and lower common-mode voltage, in comparison to the conventional two-level voltage source inverters. Therefore, the size and cost of the harmonic and EMI filters will be dramatically reduced. There are several types of multilevel inverters, such as neutral-point-clamped (NPC) inverters, cascaded H-bridge inverters, flying capacitor inverters, modular multilevel converters, as well as numerous derivatives of these topologies [98], [99]. Each multilevel inverter topology has its pros and cons, depending on the specific HRES applications and power mission profiles. The selection of the inverter topology requires comprehensive performance analysis by concurrently considering the efficiency, cost, power density, and reliability.

The T-type converter is one of the advanced NPC converter configurations that have the benefits of reduced number of switching elements and higher efficiency compared to conventional I-type NPC converter [100]. The 3-level I-type NPC inverter (3L-INPCI) and 3-level T-type NPC inverter(3L-TNPCI) are the most extensively utilized topologies for grid-tied renewable energy applications. The circuit architecture of the 3L-INPCI is illustrated in Fig. 27. The clamping diodes linked to the neutral point enable producing a zero-voltage level, with which the three different output voltage levels are obtained. The 3L-TNPCI excludes the clamping diodes from the topology, as shown in Fig. 28. The inner switches (S_2 and S_3) are associated with the neutral point of the DC bus, blocking half of the DC-bus voltage. Therefore, the breakdown voltages of inner switches (S_2 and S_3) can be half of these with the outer switches (S_1 and S_4). In comparison with the 3L-INPCI, the 3L-TNPCI has the leverage of shorter commutation loops and reduced number of switches due to no clamping diodes.

The diode clamped, flying capacitor (FC), and cascaded H-bridge (CHB) topologies are the most frequently utilized multilevel inverter (MLI) configurations in grid-interfaced RE systems. These three MLI topologies are considered as the classic MLI topologies, and they are widely employed in industries due to their common advantages, including lower harmonic distortion, higher voltage withstanding capability,

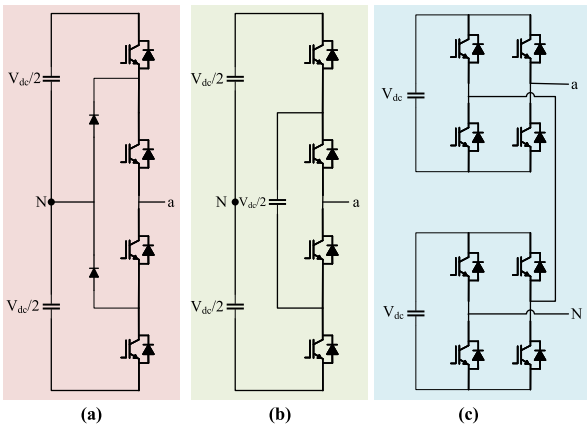

FIGURE 29. Classic multilevel inverter topologies (with one phase shown). (a) Three level diode clamped. (b) Three level flying capacitor. (c) Five level cascade H-bridge [112].

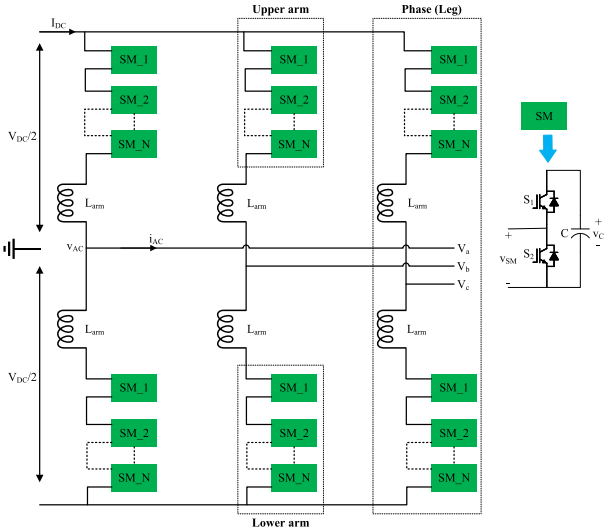

FIGURE 30. The topology of a modular multilevel converter (MMC) [102].

lower common mode voltage, and lower dv/dt in the output waveforms [101]. The configuration of a single-phase leg of these three topologies is depicted in Fig. 29. The modular multilevel converter (MMC) is another popular MLI topology that has received increasing attention for renewable energy integration due to its superior features such as modularity, scalability, high efficiency, and high output waveform quality [102]. The general topology of an MMC is illustrated in Fig. 30. The submodule (SM) can be either a half-bridge or full-bridge circuit, depending on the performance requirements. Unlike half-bridge MMC, full-bridge MMC can be controlled to isolate and tolerate a DC short-circuit fault, which is preferred for safety-critical HRES applications, while at relative higher cost due to the larger number of power devices [103]. Furthermore, based on the number of employed DC sources, the classic MLI topologies can be classified into two main groups, as shown in Fig. 31. The classic MLI configurations have been thoroughly analyzed in the literature, and

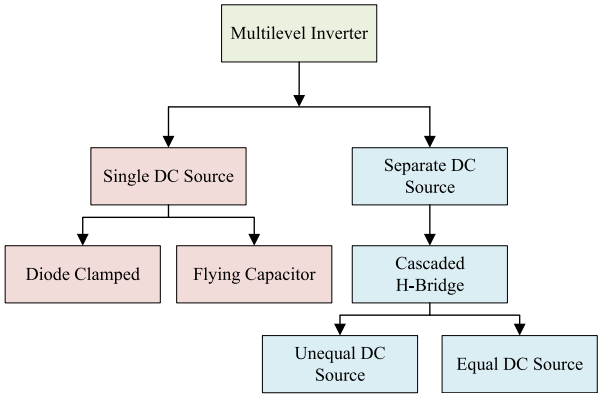

FIGURE 31. Multilevel inverter classification [112].

each has its own set of benefits and drawbacks. Here, a comparison between the classic MLI topologies is contemplated in terms of the advantages and disadvantages, as illustrated in Table 7 [104]–[108]. In the Table 7, the common advantages with MLI such as lower harmonic distortion and lower common-mode voltage are excluded, and only their unique characteristics are summarized.

Recent trends in MLI have emphasized lowering the number of switches, DC supplies, and gate driver circuits while improving power quality and fault tolerant capability in order to make them more cost-effective for grid-connected HRES applications [109]. As a result, various hybrid topologies have been developed in recent years, most of which are derived from classical topologies in order to meet high grid code standards and power quality issues while remaining cost-effective. As previously stated, based on the specific HRES applications and power mission profiles, each MLI topology has its own pros and cons. As a result, selecting an inverter topology requires a thorough performance evaluation that takes into account efficiency, cost, power density, and reliability all at the same time. Despite the fact that each MLI faces distinct challenges, the CHB families appeared to be the most suitable topology for HRES application since they provide modularity, reliability, grid support, and high power density within a reasonable range [110]. However, more improvements are required for the CHB topology to guarantee the desired performance.

E. GRID COUPLED INVERTER CONTROLLER

In the grid-connected inverter control architecture, the grid synchronization to power flow management and pulse width modulation (PWM) of the inverter is occurred. This control topology employed an outer DC-link voltage control loop and an inner current control loop to secure decoupled regulation of active and reactive power components. The grid voltage-oriented reference frame utilized for transformations deploys the phase angle provided by instantaneous voltage measurements. The voltage control loop is responsible for maintaining the DC bus voltage and providing the active power current reference to the internal current loop. The current control

TABLE 7 Summarized Advantages and Disadvantages of Classical topologies [104]–[108]

Topology	Advantages	Disadvantages
Diode-Clamped	• Single DC source (no requirements for multiple isolated DC sources). • Switches experience less voltage stress. • Capable of pre-charging the capacitors as a group. • Straightforward control mechanism. • Capability for fault-tolerant operation.	• Uneven semiconductor loss distribution. • DC-bus neutral point voltage floating. • The complexity of voltage balancing circuit. • Increased number of clamping-diodes as the level increased. • Issues with balancing and stabilizing the DC voltage of the capacitor.
Flying Capacitors	• Single DC source (no requirements for multiple isolated DC sources). • Extra ride through capability during power outage. • Appropriate switching combination for balancing different voltage levels.	• High number of clamping capacitors which may cause reliability degradation in harsh environment. • Lower power density at low-frequency operation due to the size of the flying capacitors. • Unbalanced voltage among clamping capacitors. • High complexity of the voltage balancing circuit. • Packaging becomes more complex as the number of voltage levels increases.
Cascaded H-Bridge	• Good modularity. • Easy to extend it to higher levels by stacking up. • No need for extra diodes and capacitors. • Symmetric and asymmetrical topology options.	• More gate driver circuits are required. • It requires multiple isolated DC sources to increase the output voltage. • Switches must have a blocking voltage equal to the input voltage.
MMC	• Modularity and scalability. • Absence of additional bulky capacitors on the DC bus. • Fault tolerance for full-bridge MMC. • SM modules are composed of power devices with low voltage ratings at low cost.	• SM capacitor voltage balancing algorithm is required. • Control strategy needs to be implemented to reduce the AC components of the circulating currents under fixed-frequency operation. • Additional circuit arrangements are required to control the SM capacitor voltage ripple at low frequencies.

loop, based on the active power current reference and reactive power current reference, yields the appropriate voltage reference signals. The desired voltage reference signals realized from the current controller are then employed to provide PWM pulses for the semiconductor switches in the inverter.

Nowadays, inverter-based resources are becoming an inevitable part of AC power systems due to the rapid advancement of hybrid PV-Wind grid integration. Inverter-based resources utilized in the HRES framework are responsible for providing active and reactive power to the grid. They can be categorized into two main groups: grid following inverter and grid forming inverter. The main discrepancy between the grid-forming and grid-following is the synchronization approach that gives the correct rotation in the abc/dq transformation.

To this date, the grid following inverter is dominated where a phase locked loop (PLL) is employed to align with the grid voltage at the point of common coupling (PCC) of the converter. Therefore, it follows the measured voltage by aligning and utilizing the measured voltage as a reference. As a result, the grid following inverter is not expected to respond to grid frequency variations. This specific grid following characteristic resembles a current source. On the other hand, the primary objective of the grid forming inverter is regulating the voltage and frequency of the grid. The control of converters should be restructured from a grid-following to a grid-forming control to avoid the challenges associated with low inertia. In this way, it can provide damping to frequency variations and whose character is more similar to that of a synchronous machine. This is feasible since the grid forming system generates its own internal voltage reference angle based on the output power

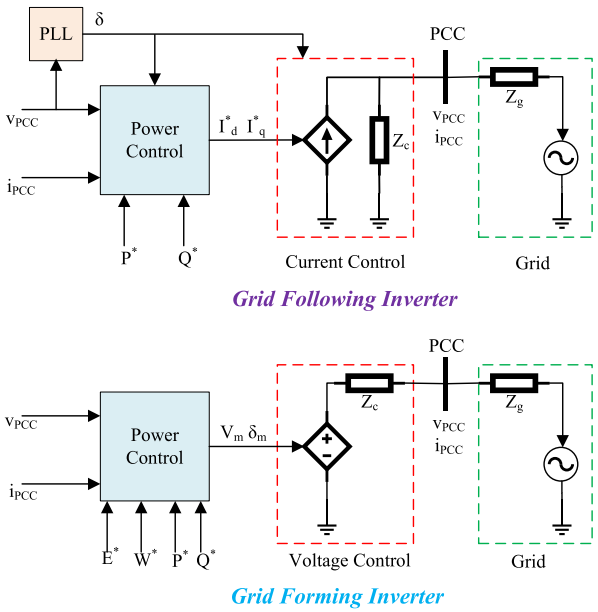

FIGURE 32. Control working principles: (a) Grid Following Inverter (Top), (b) Grid Forming Inverter (Bottom) [113], [114].

of the converter. A simplified representation of the working principles of the grid following inverter and grid forming inverter is documented in Fig. 32.

F. FILTER TOPOLOGIES FOR HRES

High-frequency switching of power converters in the HRES framework produce considerable harmonics in the systems.

Typically, for commercial and utility-scale power converters, the switching frequencies between 2 to 15 kHz can generate high-order harmonics that is responsible for inducing grid stability and harmonics issues. In general, a passive filter needs to be employed to mitigate or eliminate the harmonics around multiplies of the switching frequency. Likewise, there are several factors to be concurrently considered during the filter development, namely, attenuation ratio, voltage drop, losses, cost, weight, and volume [115].

Different circuit topologies of the grid-connected filter, such as L-filter, L-C filter, and L-C-L filter, are analyzed in the literature. The most essential features—harmonic attenuation, system dynamics, and decoupling between the filter and grid impedance—are discussed while comparing different types of filter configurations. Due to its simple structure, the L-filter can easily be implemented. However, a high value of inductance or higher switching frequency needs to be selected for reducing the harmonics around the switching frequency. As a consequence, the system dynamic response may become sluggish, and the switching losses in the semiconductor power devices may increase significantly. Although the L-C filter has satisfactory performance in voltage-current conversion, the damping of the high-frequency noise has been a challenge.

In the L-C-L filter configuration, the damping of the high-frequency noise is improved due to its extra inductance. In addition, the capacitor in the L-C-L filter is not exposed to line current distortion at the fundamental frequency, unlike the L and L-C filters [116]. The utilization of the L-C-L filter in the HRES framework provides several advantages, i.e., relatively low switching frequency requires for a given harmonic attenuation, reduces the grid current distortion, decreases the reactive power production, and so on [117], [118].

The LCL filter is a third-order filter with a $-60\ db/decade$ attenuation that produces a resonance peak. Therefore, the LCL filter must be designed meticulously according to the parameters of the inverter. Several attributes, such as current ripple, filter size, and switching ripple attenuation, must be addressed while designing an LCL filter. The design approach of the LCL filter is documented in [111].

The first step in the procedure of designing LCL filter parameters is the estimation of the base impedance (Z_b) and base capacitance (C_b) values as expressed below:

$$Base\ impedance, Z_b = \frac{V_g^2}{P_n} \tag{20}$$

$$Base\ capacitance, C_b = \frac{1}{2 \times \pi \times f_g \times Z_b} \tag{21}$$

where V_g is the line to line RMS voltage (inverter output), P_n is the rated active power, and f_g is the grid frequency.

The next step in computing the filter components is the design of the inverter side inductance (L_i), which can be indicated as:

$$L_i = \frac{V_{DC}}{16 \times f_{sw} \times \Delta I_L} \tag{22}$$

where V_{DC} is the DC bus voltage, f_{sw} is the switching frequency, and ΔI_L is the current ripple specified by:

$$\Delta I_L = (1\% - 10\%)\frac{P_n \times \sqrt{2}}{V_g} \tag{23}$$

Then, the filter capacity (C_f) is calculated as a multiplication of C_b by accounting the maximal power factor variation accepted by the grid 5%.

$$C_f = 0.05 \times C_b \tag{24}$$

The grid side inductance (L_g) can be determined as:

$$L_g = r \times L_i \tag{25}$$

where r is the ratio between the L_i and L_g.

The final step in the design is to regulate the resonant frequency (f_{res}) of the filter. Since the filter must have enough attenuation in the f_{sw} of the inverter, the f_{res} should be far above the grid frequency f_g and lower than the switching frequency f_{sw}.

$$f_{res} = \frac{1}{2\pi} \times \sqrt{\frac{L_i + L_g}{L_i \times L_g \times C_f}} \tag{26}$$

$$10 f_g \leq f_{res} \leq 0.5 f_{sw} \tag{27}$$

The filter capacitor (C_f) should be included with an in series connected resistor to diminish oscillations and unstable states of the filter. The value of the damping resistor (R_d) can be expressed as:

$$R_d = \frac{1}{3 \times 2 \times \pi \times f_{res} \times C_f} \tag{28}$$

VI. HRES OPTIMIZATION

The primary objective of using optimization techniques in HRES is to achieve superior overall performance as well as to meet grid requirements and constraints. It is crucial to implement an systematic optimization algorithm to solve the optimal solution which provides the least annual cost as well as fulfilling the requirements. Recent survey has indicated that there are different types of optimization algorithms used by the researchers for HRES, such as the genetic algorithm (GA), the particle swarm optimization (PSO), the shuffled frog leaping algorithms, etc. [119]. Constrained by system cost, efficiency target, and local weather conditions, a systematic sizing optimization method will be of paramount importance for HRES. Table 8 presents a summary of the analysis and sizing constraints employed for optimum sizing of the wind-solar HRES.

Furthermore, the widely utilized modelling and optimization approaches for the HRES can be categorized as: classical algorithms, metaheuristic methods, and hybrid of two or more optimization techniques. The differential calculus manner is used in the classical optimization algorithm to seek optimum solutions for differentiable and continuous functions. Therefore, it exhibits limited capabilities for applications whose objective functions are not continuous and/or

TABLE 8 **Optimization Algorithms of "Wind+Solar" HRES**

Ref.	Optimization Technique	Optimization Constraints	Highlights
[79]	GA	Economic	Satisfy the load demand under all conditions.
[124]	GA	Minimum annualized cost; LPSP	Good optimization performance; Relationships between the system reliability and configurations are evaluated.
[125]	Multi-objective GA	LPSP; Annualized cost	Optimal sizing; Correlations between the cost of the optimal configuration and load profile are assessed.
[126]	PSO	Total cost	Address the equality constraints for power balance; Achieve the lowest accumulated cost.
[127]	PSO	Techno-socio-economic	Optimal sizing; System reliability evaluation is carried out using an analytical approach.
[128]	Multi-objective PSO	Reliability	Produce appropriate sizing of the HRES components for each location; Enhancing energy access for remote locations.
[56]	Forever power	Reliability; Cost; Environmental benefit	Economic analysis is carried out to seek the most feasible combination of the HRES components.
[70]	GA	PV array capacity; WT numbers; ESS numbers	Optimal sizing; Relationships between the HRES power fraction and the cost of energy are investigated.
[10]	Iterative filter selection	Minimization of unutilized surplus power	Yield minimum total cost and maximum reliability.
[21]	PSO	Economic and technical indexes	Minimize the life-cycle cost; Optimal capacity of the HRES configuration.
[129]	Iterative	Deficiency of power supply probability; Unutilized energy probability; Levelized energy cost	Optimize the size of HRES for a specific location.
[48]	PSO	Economic and technical	Minimize the annualized cost; Improve the reliability index.
[21]	PSO	Economic and technical	Minimize the life-cycle cost; The influence of the optimal capacity of HRES on life-cycle cost is investigated.
[130]	PSO	Minimize the total cost	Reduce the time required to find the optimum solution.
[131]	OptQuest	Loss of load probability	Optimum sizes of the HRES components are investigated under various auxiliary energy unit costs.
[132]	GA	LPSP	Minimize the annualized cost of the HRES; Five decision variables are evaluated for optimal sizing of the HRES.
[133]	Multi-objective PSO	Net present cost; CO_2 emission	Lower net present cost compared to HOMER.
[134]	Multi-objective GA	Techno-economic approach; CO_2 emission	The HRES optimized while considering its size, cost, and availability criteria.
[135]	LPSP	Reliability; Power quality; loss of supply	The performance of the HRES is evaluated based on cost and reliability.
[136]	Iterative	Techno-Economic	The WT-PV- Battery combination in the HRES is found to be a more cost-effective scheme compared with other hybrid systems.
[137]	Iterative	Deficiency of power supply probability; Levelized unit electricity cost	Optimal sizing of the HRES components while fulfilling system reliability requirements.
[138]	Modified PSO	Optimal sizing	Faster convergence speed; Shorter computational time.
[139]	PSO	Total annual cost	The performance of different PSO variants are evaluated for optimal sizing of the HRES components; PSO with constriction factor is found to be more promising than other variants.
[140]	Multi-objective PSO	Annualized cost; Loss of load expected; Loss of energy expected	Reduce computation time; Technique for reliability evaluation of the HRES is investigated.
[141]	PSO	Total area occupied by the PV and WT; Number of batteries	Minimize the life cycle cost with a certain level of system reliability; Adaptive inertia weight-based PSO provides more promising results than the other variants.
[142]	GA	Minimization of life-cycle cost; Minimization of pollutant emissions	Optimal sizing of the HRES components.
[143]	GA	Minimization of life-cycle cost, CO_2 emissions, and dump energy	Five different types of HRES configurations are investigated for a typical residential load profile to minimize the life-cycle cost of the HRES.
[144]	Improved GA	Service life of the HRES	Better convergence speed than the standard GA.
[145]	Artificial bee swarm optimization	Minimizing the annual cost; LPSP	Artificial bee swarm optimization technique utilizes the stochastic rules to escape local optima and find the global solution.
[146]	GA	Minimizing the unmet load	The user socio-demographic profile is investigated for optimal sizing of the HRES components.
[147]	Curve fitting - PSO	Minimizing the annual cost	Hourly dispatching scheme of the HRES; Optimal scaling of the HESS; Economic analysis of the HESS.

TABLE 9 Comparative Comparison Among the Commonly Used Optimization Techniques for HRES

Techniques	Algorithms	Advantages	Disadvantages
Classical	Linear programming model	Performs stochastically in reliability and economic analysis.	Energy delivery capability is severely affected by failure any of the RE sources to function effectively.
Classical	Nonlinear programming model	Enables solving complex problems with simple operations.	Increases the required number of iterations as well as computational burden of the problem.
Classical	Dynamic programming	Competent to address the complexity of large systems.	Implementation becomes complex and confusing due to high number of recursive functions.
Metaheuristic	GA	Efficient finding an optimal solution to a given problem.	Might converge in local optima if it is not initialized or designed perfectly.
Metaheuristic	PSO	Efficacious in solving the scattering and optimization problems.	Requires considerable modifications due to its complex and conflicted nature.
Metaheuristic	Simulated annealing (SA)	Independent from initial starting condition; Computer memory requirement is minimal.	Might accept an inferior solution based upon a probabilistic measure.
Metaheuristic	Ant colony (AC)	High convergence speed.	Requires long-term memory space.
Hybrid	PSO-Differential evolution; Monte Carlo simulation (MCS)-PSO; SA-Tabu search; Hybrid iterative-GA; Artificial neural fuzzy inference system; Artificial neural network-GA-MCS.	Ameliorate the overall performance of the optimization.	Increases the coding and design complexity; Might converge into suboptimal solution.

differentiable [120]. Metaheuristic strategies have the potential to provide efficient, accurate, and optimal solutions, and it is extensively employed for optimizing the complex HRES. Metaheuristic approaches are nature-based, and their evolutions are based on the behavior of nature [121], [122]. In the hybrid techniques, two or more optimization approaches are combined to overcome the limitations of the individual strategies mentioned above. Consequently, it can provide more effective and reliable solutions for HRES [123]. The attributes of these optimization techniques are synopsized in Table 9.

The various criteria are contemplated in the literature for optimal sizing of the HRES can be mainly categorized as economic and technical. Economic criteria are employed to minimize the expenditure of the HRES. The cost optimization of the HRES, which objective is to seek the compromise solution between the costs and benefits, including minimizing energy cost, net present cost, and any other costs associated with the HRES. On the other hand, technical criteria deal with the reliability, efficiency, and environmental benefits of the HRES. The objective of the technical criteria fulfills the desired reliability levels based on loss of power supply probability or loss of load probability, curtailing cost/efficiency ratio, minimizing carbon emissions and maximizing power.

VII. BENEFITS AND CHALLENGES OF HRES

To sum up, the advantages of the HRES can be highlighted as follows:

- Continuous power supply.
- Utilize the RE sources in best way.
- Low maintenance cost.
- High efficiency.
- Load is supplied in the most optimal way.
- Improves the dispatch flexibility.
- Greater balance in energy supply.
- Yield greater economic and environmental returns.
- Reduces negative effects associated with burning fossil fuels.
- HRES can be synchronized to ameliorate the RE converter infrastructure.
- Enhance the system reliability.
- Decreases lifecycle costs for peaky loads or growing fixed loads.
- System energy service is enhanced.
- Truncates downtime during repairs or routine maintenance.
- Nearly zero pollutant emissions especially for PV-Wind-Energy storage HRES architecture.
- Relived transmission and distribution congestion.
- Improved power quality.
- Provides more flexibility for future extension and growth.

Even though the HRES has come a long way in terms of research and development, there are still some impediments in terms of its efficiency and optimal utilization. The challenges associated with the HRES faced by practitioners can be summarized as:

- The HRES demands innovative technology to harness the optimal power from the RE sources.
- The poor efficiency of HRES is a significant hindrance in encouraging its deployment.
- Since the high capital cost leads to a prolonged payback time, the manufacturing expenditure of RE sources requires a substantial reduction.
- The power electronic devices interfaced with HRES should be a minimal amount of power loss.
- Geography plays a prominent role in the HRES deployment.
- Due to the high installation expenditure, government incentive policies are required to make the HRES economically viable.

- The energy storage technologies deserve more research attention and efforts to ease their durability and performance.
- Real-time energy management and robust communication between the respective energy sources of the HRES require to be ameliorated through cutting-edge investigation.
- Systematic approaches and standardization, e.g., IEEE Standard 1547, are demanded effective and safe deployment of the HRES.
- As the new advanced semiconductor devices such as silicon carbide and gallium nitride become available, research efforts are required to integrate them into the evolving HRES.
- System reliability and energy sustainability are needed to be improved to the maximum extent possible.

VIII. FUTURE TRENDS OF HRES

In the future, operators would like RE plants to have the ability to operate more like traditional power plants in terms of capacity value, dispatchability, ancillary services, and reliability. As higher HRES capacity is connected to the power grid, it is expected that integration technology for high levels of HRES penetration will be an important research area in the following decade. Here, the future trends of the HRES are outlined as follows:

- Further advances in wind-solar technologies will significantly reduce the cost of HRES. As a result, HRES will be more cost-effective in the future. Aside from the expense, the environmental advantages are likely to make this hybrid system more widely used and accepted.
- A modern control technique can be employed to ensure optimal resource allocation based on load demand and RE resource forecast. Correspondingly, the total operating cost of HRES will be reduced substantially.
- Artificial intelligence as part of the energy management system has the potential to improve HRES operation.
- Advanced control methods implemented in a centralized system controller can ameliorate the performance of modular hybrid systems.
- Advanced research in the control and operation of HRES should be performed in the areas of grid code compliance and the potential to provide ancillary services to the grid.
- Developing an RE optimization model or toolset to survey and analyze market and resource conditions in order to assess the performance and cost of HRES.
- Evaluate HRES-specific design challenges and opportunities, e.g., economies of scale, technological innovation.
- Standard guidelines on the forecasting of hybrid power plant energy in commitment and dispatch operations must be defined for utilities.
- Most HRES plant designs are still in the early stages of development, which means that their long-term viability in terms of energy and capacity has yet to be established.
- Investigate various system architectures (AC coupled, DC coupled) and innovations related to inverters within the HRES.
- During the implementation of the HRES project, a systematic approach for optimizing the sizing of different assets and their layout to meet land constraints must be devised.
- As the penetration of the HRES increases, specifications for transient voltage and frequency become more critical. As a result, many countries' grid codes will need to be updated to accommodate the integration of the HRES generation and maintain a stable operation.
- The ESS becomes an indispensable component by strongly supporting ramp control and frequency regulation in HRES deployment. As a result, more detailed grid codes for ESS are expected in the future, including inertia emulation, power oscillation damping, and voltage control.
- Advanced weather forecasting techniques will reduce the uncertainty of HRES generation considerably and avoid HRES energy curtailment substantially.
- Both the sensitivity and reliability assessments of any proposed HRES configuration should be carried out.
- Develop a paradigm that would enable a feedback mechanism between end-users and grid operators to further improve the system's reliability and flexibility.
- There should be a minimal amount of power loss in the power electronic devices while interfacing the HRES to the utility.

IX. CONCLUSION

In this paper, a comprehensive review of existing wind-solar hybrid renewable energy resources is conducted, in which the system modeling, power converter configurations, and the optimal design algorithms are reviewed. The basic mathematical modeling of PV and WT, and the degradation model of batteries and supercapacitors are discussed in this study. A critical review of different HESS topologies is presented. A comparative study on different power converter configurations employed in the wind-solar HRES is also reported. Commonly used optimization algorithms in the literature for optimizing the wind-solar HRES system are analyzed and summarized. Although considerable accomplishments have been achieved over the years on various HRES, a comprehensive review helps to identify and fulfill the technical gaps for improving the future HRES.

REFERENCES

[1] W. Ur Rehman *et al.*, "The penetration of renewable and sustainable energy in Asia: A state-of-the-art review on net-metering," *IEEE Access*, vol. 8, pp. 170364–170388, 2020.

[2] D. Gielen, F. Boshell, D. Saygin, M. D. Bazilian, N. Wagner, and R. Gorini, "The role of renewable energy in the global energy transformation," *Energy Strategy Rev.*, vol. 24, pp. 38–50, 2019.

[3] S. Koebrich, T. Bowen, and A. Sharpe, "2018 renewable energy data book," U. S. Dept. Energy, Office of Energy Efficiency & Renewable Energy, 2018.

[4] "Renewable energy market update 2021," IEA, Paris, [Online]. Available: https://www.iea.org/reports/renewable-energy-market-update-2021

[5] W. Thomas, "FY22 budget outlook: DOE applied energy RD&D," Amer. Inst. of Phys., Accessed: Nov. 5, 2021, [Online]. Available: https://www.aip.org/fyi/2021/fy22-budget-outlook-doe-applied-energy-rdd

[6] S. Ray, "Renewables account for most new U. S. electricity generating capacity in 2021," U.S. Energy Inf. Admin. (EIA), Accessed: Nov. 11, 2021, [Online]. Available: https://www.eia.gov/todayinenergy/detail.php?id=46416

[7] P. L. Joskow, "Challenges for wholesale electricity markets with intermittent renewable generation at scale: The US experience," *Oxford Rev. Econ. Policy*, vol. 35, no. 2, pp. 291–331, 2019.

[8] B. K. Sovacool, "The intermittency of wind, solar, and renewable electricity generators: Technical barrier or rhetorical excuse?," *Utilities Policy*, vol. 17, no. 3-4, pp. 288–296, 2009.

[9] P. Denholm *et al.*, "Overgeneration from solar energy in California: A field guide to the duck chart," Nat. Renewable Energy Lab., Tech. Rep. NREL/TP-6A20-65023, 2015. Accessed: Nov. 7, 2021. [Online]. Available: https://nrel.gov/publications

[10] S. Hussain, R. Al-ammari, A. Iqbal, M. Jafar, and S. Padmanaban, "Optimisation of hybrid renewable energy system using iterative filter selection approach," *IET Renewable Power Gener.*, vol. 11, no. 11, pp. 1440–1445, 2017.

[11] A. Andreas and T. Stoffel, "NREL solar radiation research laboratory (SRRL): Baseline measurement system (BMS)," Golden, Colorado (Data); NREL Report No. Tech. Rep. DA-5500-56488, 1981.

[12] R. A. Badwawi, M. Abusara, and T. Mallick, "A review of hybrid solar PV and wind energy system," *Smart Sci.*, vol. 3, no. 3, pp. 127–138, 2015.

[13] M. A. Alotaibi and A. M. Eltamaly, "A smart strategy for sizing of hybrid renewable energy system to supply remote loads in Saudi Arabia," *Energies*, vol. 14, no. 21, 2021, Art. no. 7069.

[14] H. K. Trabish, "Solar wind storage developers 'gearing up' as hybrid projects edge to market," Utility Dive, Jul. 2019. Accessed: Sep. 30, 2020. [Online]. Available: https://www.utilitydive.com

[15] E. Bellini, "Danish fjord to host 400 MW of solar," *PV Mag. Int.* Mar. 2020, Accessed: Sep. 30, 2020. [Online]. Available: https://www.pv-magazine.com

[16] R. Walton, "NextEra inks 700 MW wind solar battery project, largest in the US," *Utility Dive*, Jul. 2019, Accessed: Sep. 30, 2020. [Online]. Available: https://www.utilitydive.com

[17] J. L. Bernal-Agustín and R. Dufo-López, "Simulation and optimization of stand-alone hybrid renewable energy systems," *Renewable Sustain. Energy Rev.*, vol. 13, no. 8, pp. 2111–2118, 2009.

[18] S. Munuswamy, K. Nakamura, and A. Katta, "Comparing the cost of electricity sourced from a fuel cell-based renewable energy system and the national grid to electrify a rural health centre in India: A case study," *Renewable Energy*, vol. 36, no. 11, pp. 2978–2983, 2011.

[19] C. Li, X. Zhu, G. Cao, S. Sui, and M. Hu, "Dynamic modeling and sizing optimization of stand-alone photovoltaic power systems using hybrid energy storage technology," *Renewable Energy*, vol. 34, no. 3, pp. 815–826, 2009.

[20] G. Graditi, S. Favuzza, and E. R. Sanseverino, "Technical, environmental and economical aspects of hybrid system including renewables and fuel cells," in *Proc. Int. Symp. Power Electron., Elect. Drives, Automat. Motion*, 2006, pp. 531–536.

[21] C. Zhu, F. Liu, S. Hu, and S. Liu, "Research on capacity optimization of PV-Wind-Diesel-Battery hybrid generation system," in *Proc. Int. Power Electron. Conf.*, 2018, pp. 3052–3057.

[22] A. M. Eltamaly and A. A. Al-Shamma'a, "Optimal configuration for isolated hybrid renewable energy systems," *J. Renewable Sustain. Energy*, vol. 8, no. 4, 2016, Art. no. 045502.

[23] M. H. Nehrir *et al.*, "A review of hybrid renewable/alternative energy systems for electric power generation: Configurations, control, and applications," *IEEE Trans. Sustain. Energy*, vol. 2, no. 4, pp. 392–403, Oct. 2011.

[24] K. Anoune, M. Bouya, A. Astito, and A. B. Abdellah, "Sizing methods and optimization techniques for PV-Wind based hybrid renewable energy system: A review," *Renewable Sustain. Energy Rev.*, vol. 93, pp. 652–673, 2018.

[25] L. Lu, H. Yang, and J. Burnett, "Investigation on wind power potential on Hong Kong islands–An analysis of wind power and wind turbine characteristics," *Renewable Energy*, vol. 27, no. 1, pp. 1–12, 2002.

[26] R. Carnegie, D. Gotham, D. Nderitu, and P. Preckel, "Utility scale energy storage systems benefits, applications, and technologies," State Utility Forecasting Group, Tech. Rep., Jun. 2013.

[27] "SCE unveils largest battery energy storage project in North America," Edison International, Accessed: Sep. 30, 2020. [Online]. Available: https://newsroom.edison.com

[28] H. Chen, T. N. Cong, W. Yang, C. Tan, Y. Li, and Y. Ding, "Progress in electrical energy storage system: A critical review," *Prog. Natural Sci.*, vol. 19, no. 3, pp. 291–312, 2009.

[29] B. Zakeri and S. Syri, "Electrical energy storage systems: A comparative life cycle cost analysis," *Renewable Sustain. Energy Rev.*, vol. 42, pp. 569–596, 2015.

[30] S. K. Kollimalla, M. K. Mishra, and N. L. Narasamma, "Design and analysis of novel control strategy for battery and supercapacitor storage system," *IEEE Trans. Sustain. Energy*, vol. 5, no. 4, pp. 1137–1144, Oct. 2014.

[31] B. R. Ravada, N. R. Tummuru, and B. N. L. Ande, "Photovoltaic-wind and hybrid energy storage integrated multisource converter configuration-based grid-interactive microgrid," *IEEE Trans. Ind. Electron.*, vol. 68, no. 5, pp. 4004–4013, May 2021.

[32] A. Kuperman and I. Aharon, "Battery-ultracapacitor hybrids for pulsed current loads: A review," *Renewable Sustain. Energy Rev.*, vol. 15, no. 2, pp. 981–992, 2011.

[33] T. Ma, H. Yang, and L. Lu., "Development of hybrid battery-supercapacitor energy storage for remote area renewable energy systems," *Appl. Energy*, vol. 153, pp. 56–62, 2015.

[34] R. A. Dougal, S. Liu, and R. E. White, "Power and life extension of battery-ultracapacitor hybrids," *IEEE Trans. Compon. Packag. Technol.*, vol. 25, no. 1, pp. 120–131, Mar. 2002.

[35] J. P. Zheng, T. R. Jow, and M. S. Ding, "Hybrid power sources for pulsed current applications," *IEEE Trans. Aerosp. Electron. Syst.*, vol. 37, no. 1, pp. 288–292, Jan. 2001.

[36] Z. Song, H. Hofmann, J. Li, X. Han, X. Zhang, and M. Ouyang, "A comparison study of different semi-active hybrid energy storage system topologies for electric vehicles," *J. Power Sources*, vol. 274, pp. 400–411, 2015.

[37] Y. Wang, W. Wang, Y. Zhao, L. Yang, and W. Chen, "A fuzzy-logic power management strategy based on Markov random prediction for hybrid energy storage systems," *Energies*, vol. 9, p. 25, 2016.

[38] W. Li, G. Joós, and J. Bélanger, "Real-time simulation of a wind turbine generator coupled with a battery supercapacitor energy storage system," *IEEE Trans. Ind. Electron.*, vol. 57, no. 4, pp. 1137–1145, Apr. 2010.

[39] L. Gao, R. A. Dougal, and S. Liu, "Power enhancement of an actively controlled battery/ultracapacitor hybrid," *IEEE Trans. Power Electron.*, vol. 20, no. 1, pp. 236–243, Jan. 2005.

[40] A. Khaligh and Z. Li, "Battery, ultracapacitor, fuel cell, and hybrid energy storage systems for electric, hybrid electric, fuel cell, and plug-in hybrid electric vehicles: State of the art," *IEEE Trans. Veh. Technol.*, vol. 59, no. 6, pp. 2806–2814, Jul. 2010.

[41] A. Kuperman, I. Aharon, S. Malki, and A. Kara, "Design of a semiactive battery-ultracapacitor hybrid energy source," *IEEE Trans. Power Electron.*, vol. 28, no. 2, pp. 806–815, Feb. 2013.

[42] E. Jamshidpour, S. Saadate, and P. Poure, "Energy management and control of a stand-alone photovoltaic/ultra capacitor/battery microgrid," in *Proc. IEEE Jordan Conf. Appl. Elect. Eng. Comput. Technol.*, 2015, pp. 1–6.

[43] S. M. Lukic, S. G. Wirasingha, F. Rodriguez, J. Cao, and A. Emadi, "Power management of an ultracapacitor/battery hybrid energy storage system in an HEV," in *Proc. IEEE Veh. Power Propulsion Conf.*, 2006, pp. 1–6.

[44] J. Cao and A. Emadi, "A new Battery/UltraCapacitor hybrid energy storage system for electric, hybrid, and plug-in hybrid electric vehicles," *IEEE Trans. Power Electron.*, vol. 27, no. 1, pp. 122–132, Jan. 2012.

[45] J. J. Soon and K.-S. Low, "Optimizing photovoltaic model for different cell technologies using a generalized multidimension diode model," *IEEE Trans. Ind. Electron.*, vol. 62, no. 10, pp. 6371–6380, Oct. 2015.

[46] M. C. Cavalcanti, F. Bradaschia, A. J. do Nascimento, G. M. Azevedo, and E. J. Barbosa, "Hybrid maximum power point tracking technique for PV modules based on a double-diode model," *IEEE Trans. Ind. Electron.*, vol. 68, no. 9, pp. 8169–8181, Sep. 2020.

[47] H. Patel and V. Agarwal, "Maximum power point tracking scheme for PV systems operating under partially shaded conditions," *IEEE Trans. Ind. Electron.*, vol. 55, no. 4, pp. 1689–1698, Apr. 2008.

[48] F. Jahanbani Ardakani, G. Riahy, and M. Abedi, "Design of an optimum hybrid renewable energy system considering reliability indices," in *Proc. 18th Iranian Conf. Elect. Eng.*, 2010, pp. 842–847.

[49] M. Yousefi, A. Hajizadeh, and M. N. Soltani, "A comparison study on stochastic modeling methods for home energy management systems," *IEEE Trans. Ind. Informat.*, vol. 15, no. 8, pp. 4799–4808, Aug. 2019.

[50] A. M. Muzathik, "Photovoltaic modules operating temperature estimation using a simple correlation," *Int. J. Energy Eng.*, vol. 4, pp. 151–158, Aug. 2014.

[51] J. A. Kratochvil, W. E. Boyson, and D. L. King, "Photovoltaic array performance model," Sandia Nat. Laboratories, Tech. Rep. No. SAND2004-3535, 2004.

[52] P. Gilman, A. Dobos, N. DiOrio, J. Freeman, S. Janzou, and D. Ryberg, "Sam photovoltaic model technical reference update," NREL: Golden, CO, USA, Tech. Rep. NREL/TP-6A20-67399, Mar. 2018.

[53] C. Bueno and J. Carta, "Technical-economic analysis of wind-powered pumped hydrostorage systems. Part I: Model development," *Sol. Energy*, vol. 78, no. 3, pp. 382–395, 2005.

[54] F. O. Hocaoğlu, N. ÖmerGerek, and M. Kurban, "A novel hybrid (Wind-Photovoltaic) system sizing procedure," *Sol. Energy*, vol. 83, no. 11, pp. 2019–2028, 2009.

[55] D. M. Vijay, B. Singh, and G. Bhuvaneswari, "Sensorless SynRG based variable speed wind generator and single-stage solar PV array integrated grid system with maximum power extraction capability," *IEEE Trans. Ind. Electron.*, vol. 67, no. 9, pp. 7529–7539, Sep. 2019.

[56] S. H. Alalwan and J. W. Kimball, "Optimal sizing of a wind/solar/battery hybrid microgrid system using the forever power method," in *Proc. 7th Annu. IEEE Green Technol. Conf.*, 2015, pp. 29–35.

[57] B. Ould Bilal, V. Sambou, P. A. Ndiaye, C. M. F. Kébé, and M. Ndongo, "Multi-objective design of PV-Wind-Batteries hybrid systems by minimizing the annualized cost system and the loss of power supply probability (LPSP)," in *Proc. IEEE Int. Conf. Ind. Technol.*, 2013, pp. 861–868.

[58] G. Ofualagba and E. U. Ubeku, "Wind energy conversion system-wind turbine modeling," in *Proc. IEEE Power Energy Soc. Gen. Meeting - Convers. Del. Elect. Energy 21st Century*, 2008, pp. 1–8.

[59] C. N. Bhende, S. Mishra, and S. G. Malla, "Permanent magnet synchronous generator-based standalone wind energy supply system," *IEEE Trans. Sustain. Energy*, vol. 2, no. 4, pp. 361–373, Oct. 2011.

[60] D. Verma, S. Nema, A. Shandilya, and S. K. Dash, "Maximum power point tracking (MPPT) techniques: Recapitulation in solar photovoltaic systems," *Renewable Sustain. Energy Rev.*, vol. 54, pp. 1018–1034, 2016.

[61] M. A. Ramli, S. Twaha, K. Ishaque, and Y. A. Al-Turki, "A review on maximum power point tracking for photovoltaic systems with and without shading conditions," *Renewable Sustain. Energy Rev.*, vol. 67, pp. 144–159, 2017.

[62] B. Subudhi and R. Pradhan, "A comparative study on maximum power point tracking techniques for photovoltaic power systems," *IEEE Trans. Sustain. Energy*, vol. 4, no. 1, pp. 89–98, Jan. 2013.

[63] A. R. Jordehi, "Maximum power point tracking in photovoltaic (PV) systems: A review of different approaches," *Renewable Sustain. Energy Rev.*, vol. 65, pp. 1127–1138, 2016.

[64] A. R. Reisi, M. H. Moradi, and S. Jamasb, "Classification and comparison of maximum power point tracking techniques for photovoltaic system: A review," *Renewable Sustain. Energy Rev.*, vol. 19, pp. 433–443, 2013.

[65] D.-Y. Li, Y.-D. Song, Z.-X. Gan, and W.-C. Cai, "Fault-tolerant optimal tip-speed-ratio tracking control of wind turbines subject to actuation failures," *IEEE Trans. Ind. Electron.*, vol. 62, no. 12, pp. 7513–7523, Dec. 2015.

[66] K.-H. Kim, T. L. Van, D.-C. Lee, S.-H. Song, and E.-H. Kim, "Maximum output power tracking control in variable-speed wind turbine systems considering rotor inertial power," *IEEE Trans. Ind. Electron.*, vol. 60, no. 8, pp. 3207–3217, Aug. 2013.

[67] S. M. R. Kazmi, H. Goto, H.-J. Guo, and O. Ichinokura, "A novel algorithm for fast and efficient speed-sensorless maximum power point tracking in wind energy conversion systems," *IEEE Trans. Ind. Electron.*, vol. 58, no. 1, pp. 29–36, Jan. 2011.

[68] S. Musunuri and H. Ginn, "Comprehensive review of wind energy maximum power extraction algorithms," in *Proc. IEEE power Energy Soc. Gen. Meeting*, 2011, pp. 1–8.

[69] M. A. Abdullah, A. Yatim, C. W. Tan, and R. Saidur, "A review of maximum power point tracking algorithms for wind energy systems," *Renewable Sustain. Energy Rev.*, vol. 16, no. 5, pp. 3220–3227, 2012.

[70] A. A. Al-Shamma'a and K. E. Addoweesh, "Optimum sizing of hybrid PV/wind/battery/diesel system considering wind turbine parameters using genetic algorithm," in *Proc. IEEE Int. Conf. Power Energy*, 2012, pp. 121–126.

[71] T. Kovaltchouk, H. Ben Ahmed, B. Multon, J. Aubry, and P. Venet, "An aging-aware life cycle cost comparison between supercapacitors and Li-ion batteries to smooth direct wave energy converter production," in *Proc. IEEE Eindhoven PowerTech*, 2015, pp. 1–6.

[72] J.-K. Eom, S.-R. Lee, E.-J. Ha, B.-Y. Choi, and C.-Y. Won, "Economic dispatch algorithm considering battery degradation characteristic of energy storage system with PV system," in *Proc. 17th Int. Conf. Elect. Mach. Syst.*, 2014, pp. 849–854.

[73] T. Kovaltchouk, B. Multon, H. Ben Ahmed, J. Aubry, and P. Venet, "Enhanced aging model for supercapacitors taking into account power cycling: Application to the sizing of an energy storage system in a direct wave energy converter," *IEEE Trans. Ind. Appl.*, vol. 51, no. 3, pp. 2405–2414, May 2015.

[74] X. Liu, P. C. Loh, P. Wang, and F. Blaabjerg, "A direct power conversion topology for grid integration of hybrid AC/DC energy resources," *IEEE Trans. Ind. Electron.*, vol. 60, no. 12, pp. 5696–5707, Dec. 2013.

[75] F. Dincer and M. Meral, "Critical factors that affecting efficiency of solar cells," *Smart Grid Renewable Energy*, vol. 1, no. 1, pp. 47–50, 2010.

[76] K. Krishnamurthy, S. Padmanaban, F. Blaabjerg, R. B. Neelakandan, and K. R. Prabhu, "Power electronic converter configurations integration with hybrid energy sources - A comprehensive review for state-of the-art in research," *Elect. Power Compon. Syst.*, vol. 47, no. 18, pp. 1623–1650, 2019.

[77] X. Li, D. Hui, and X. Lai, "Battery energy storage station (BESS)-based smoothing control of photovoltaic (PV) and wind power generation fluctuations," *IEEE Trans. Sustain. Energy*, vol. 4, no. 2, pp. 464–473, Apr. 2013.

[78] S. Kim, B. Kang, S. Bae, and J. Park, "Application of SMES and grid code compliance to wind/photovoltaic generation system," *IEEE Trans. Appl. Supercond.*, vol. 23, no. 3, Jun. 2013, Art. no. 5000804.

[79] M. Kalantar and S. Mousavi G., "Dynamic behavior of a stand-alone hybrid power generation system of wind turbine, microturbine, solar array and battery storage," *Appl. Energy*, vol. 87, no. 10, pp. 3051–3064, 2010.

[80] D. Wu, F. Tang, T. Dragicevic, J. C. Vasquez, and J. M. Guerrero, "A control architecture to coordinate renewable energy sources and energy storage systems in islanded microgrids," *IEEE Trans. Smart Grid*, vol. 6, no. 3, pp. 1156–1166, May 2015.

[81] E. Kabalci, "Design and analysis of a hybrid renewable energy plant with solar and wind power," *Energy Convers. Manage.*, vol. 72, pp. 51–59, 2013.

[82] S. Kim, J. Jeon, C. Cho, J. Ahn, and S. Kwon, "Dynamic modeling and control of a grid-connected hybrid generation system with versatile power transfer," *IEEE Trans. Ind. Electron.*, vol. 55, no. 4, pp. 1677–1688, Apr. 2008.

[83] L. Xu, X. Ruan, C. Mao, B. Zhang, and Y. Luo, "An improved optimal sizing method for wind-solar-battery hybrid power system," *IEEE Trans. Sustain. Energy*, vol. 4, no. 3, pp. 774–785, Jul. 2013.

[84] H. Ghoddami, M. B. Delghavi, and A. Yazdani, "An integrated wind-photovoltaic-battery system with reduced power-electronic interface and fast control for grid-tied and off-grid applications," *Renewable Energy*, vol. 45, pp. 128–137, 2012.

[85] P. Roy and J. He, "Grid-connected hybrid wind-solar farm hourly dispatching with battery and supercapacitor energy storage," in *Proc. 46th Annu. Conf. IEEE Ind. Electron. Soc.*, 2020, pp. 1831–1836.

[86] J. Hui, A. Bakhshai, and P. K. Jain, "A hybrid wind-solar energy system: A new rectifier stage topology," in *Proc. 25th Annu. IEEE Appl. Power Electron. Conf. Expo.*, 2010, pp. 155–161.

[87] W. Jiang and B. Fahimi, "Multiport power electronic interface-concept, modeling, and design," *IEEE Trans. Power Electron.*, vol. 26, no. 7, pp. 1890–1900, Jul. 2011.

[88] W. Jiang and B. Fahimi, "Multi-port power electric interface for renewable energy sources," in *Proc. 24th Annu. IEEE Appl. Power Electron. Conf. Expo.*, 2009, pp. 347–352.

[89] J. Zeng, W. Qiao, L. Qu, and Y. Jiao, "An isolated multiport DC-DC converter for simultaneous power management of multiple different renewable energy sources," *IEEE Trans. Emerg. Sel. Topics Power Electron.*, vol. 2, no. 1, pp. 70–78, Jan. 2014.

[90] Z. Qian, O. Abdel-Rahman, and I. Batarseh, "An integrated four-port DC/DC converter for renewable energy applications," *IEEE Trans. Power Electron.*, vol. 25, no. 7, pp. 1877–1887, Jul. 2010.

[91] C. Chen, C. Liao, K. Chen, and Y. Chen, "Modeling and controller design of a semiisolated multiinput converter for a hybrid PV/Wind power charger system," *IEEE Trans. Power Electron.*, vol. 30, no. 9, pp. 4843–4853, Sep. 2015.

[92] Z. Qian, O. Abdel-Rahman, H. Hu, and I. Batarseh, "A zero-voltage switching four-port integrated DC/DC converter," in *Proc. Intelec*, 2010, pp. 1–8.

[93] S. H. Hosseini, S. K. Haghighian, S. Danyali, and H. Aghazadeh, "Multi-input DC boost converter supplied by a hybrid PV/Wind turbine power systems for street lighting application connected to the grid," in *Proc. 47th Int. Universities Power Eng. Conf.*, 2012, pp. 1–6.

[94] B. Mangu, S. Akshatha, D. Suryanarayana, and B. G. Fernandes, "Grid-connected PV-Wind-battery-based multi-input transformer-coupled bidirectional DC-DC converter for household applications," *IEEE Trans. Emerg. Sel. Topics Power Electron.*, vol. 4, no. 3, pp. 1086–1095, Mar. 2016.

[95] N. K. Reddi, M. R. Ramteke, H. M. Suryawanshi, K. Kothapalli, and S. P. Gawande, "An isolated multi-input ZCS DC-DC front-end-converter based multilevel inverter for the integration of renewable energy sources," *IEEE Trans. Ind. Appl.*, vol. 54, no. 1, pp. 494–504, Jan./Feb. 2018.

[96] T. Ishikawa, "Grid-connected photovoltaic power systems: Survey of inverter and related protection equipments," *Int. Energy Agency*, pp. 1–64, 2002.

[97] M. Calais and V. G. Agelidis, "Multilevel converters for single-phase grid connected photovoltaic systems-an overview," in *Proc. IEEE Int. Symp. Ind. Electron. (Cat. No.98TH8357)*, 1998, vol. 1, pp. 224–229.

[98] K. Zeb *et al.*, "A comprehensive review on inverter topologies and control strategies for grid connected photovoltaic system," *Renewable Sustain. Energy Rev.*, vol. 94, pp. 1120–1141, 2018.

[99] B. K. Santhoshi, K. M. Sundaram, S. Padmanaban, J. B. Holm-Nielsen, and K. K. Prabhakaran, "Critical review of PV grid-tied inverters," *Energies*, vol. 12, no. 10, 2019, Art. no. 1921.

[100] M. Schweizer and J. W. Kolar, "Design and implementation of a highly efficient three-level T-type converter for low-voltage applications," *IEEE Trans. Power Electron.*, vol. 28, no. 2, pp. 899–907, Feb. 2013.

[101] P. Kala and S. Arora, "A comprehensive study of classical and hybrid multilevel inverter topologies for renewable energy applications," *Renewable Sustain. Energy Rev.*, vol. 76, pp. 905–931, 2017.

[102] M. Kurtoğlu, F. Eroğlu, A. O. Arslan, and A. M. Vural, "Recent contributions and future prospects of the modular multilevel converters: A comprehensive review," *Int. Trans. Elect. Energy Syst.*, vol. 29, no. 3, 2019, Art. no. e2763.

[103] J. He, Q. Yang, and Z. Wang, "On-line fault diagnosis and fault-tolerant operation of modular multilevel converters-a comprehensive review," *CES Trans. Elect. Mach. Syst.*, vol. 4, no. 4, pp. 360–372, 2020.

[104] N. S. Hasan *et al.*, "Reviews on multilevel converter and modulation techniques," *Renewable Sustain. Energy Rev.*, vol. 80, pp. 163–174, 2017.

[105] M. Vijeh, M. Rezanejad, E. Samadaei, and K. Bertilsson, "A general review of multilevel inverters based on main submodules: Structural point of view," *IEEE Trans. Power Electron.*, vol. 34, no. 10, pp. 9479–9502, Oct. 2019.

[106] M. Malinowski, K. Gopakumar, J. Rodriguez, and M. A. Perez, "A survey on cascaded multilevel inverters," *IEEE Trans. Ind. Electron.*, vol. 57, no. 7, pp. 2197–2206, Jul. 2009.

[107] S. Debnath, "Control of modular multilevel converters for grid integration of full-scale wind energy conversion systems," Ph.D. dissertation, Purdue Univ., West Lafayette, IN, USA, 2015.

[108] J. Wang, R. Burgos, and D. Boroyevich, "A survey on the modular multilevel converters-modeling, modulation and controls," in *Proc. IEEE Energy Convers. Congr. Expo.*, 2013, pp. 3984–3991.

[109] K. K. Gupta, A. Ranjan, P. Bhatnagar, L. K. Sahu, and S. Jain, "Multilevel inverter topologies with reduced device count: A review," *IEEE Trans. Power Electron.*, vol. 31, no. 1, pp. 135–151, Jan. 2016.

[110] S. Alotaibi and A. Darwish, "Modular multilevel converters for large-scale grid-connected photovoltaic systems: A review," *Energies*, vol. 14, no. 19, 2021, Art. no. 6213.

[111] P. Roy and J. He, "Hourly dispatching utility-scale solar PV power with megawatt multilevel grid inverter," in *Proc. IEEE Kansas Power Energy Conf.*, 2021, pp. 1–6.

[112] S. Kouro *et al.*, "Recent advances and industrial applications of multilevel converters," *IEEE Trans. Ind. Electron.*, vol. 57, no. 8, pp. 2553–2580, Aug. 2010.

[113] R. Rosso, X. Wang, M. Liserre, X. Lu, and S. Engelken, "Grid-forming converters: An overview of control approaches and future trends," in *Proc. IEEE Energy Convers. Congr. Expo.*, 2020, pp. 4292–4299.

[114] J. Rocabert, A. Luna, F. Blaabjerg, and P. Rodríguez, "Control of power converters in AC microgrids," *IEEE Trans. Power Electron.*, vol. 27, no. 11, pp. 4734–4749, Nov. 2012.

[115] A. Rockhill, M. Liserre, R. Teodorescu, and P. Rodriguez, "Grid-filter design for a multimegawatt medium-voltage voltage-source inverter," *IEEE Trans. Ind. Electron.*, vol. 58, no. 4, pp. 1205–1217, Apr. 2011.

[116] Y. Tang, P. C. Loh, P. Wang, F. H. Choo, F. Gao, and F. Blaabjerg, "Generalized design of high performance shunt active power filter with output LCL filter," *IEEE Trans. Ind. Electron.*, vol. 59, no. 3, pp. 1443–1452, Mar. 2012.

[117] J. Bauer, "Single phase voltage source inverter photovoltaic application," *Acta Polytechnica*, vol. 50, no. 4, pp. 7–11, 2010.

[118] P. Channegowda and V. John, "Filter optimization for grid interactive voltage source inverters," *IEEE Trans. Ind. Electron.*, vol. 57, no. 12, pp. 4106–4114, Dec. 2010.

[119] N. Tutkun, N. Çelebi, and N. Bozok, "Optimum unit sizing of Wind-PV-Battery system components in a typical residential home," in *Proc. Int. Renewable Sustain. Energy Conf.*, 2016, pp. 432–436.

[120] R. Siddaiah and R. Saini, "A review on planning, configurations, modeling and optimization techniques of hybrid renewable energy systems for off grid applications," *Renewable Sustain. Energy Rev.*, vol. 58, pp. 376–396, 2016.

[121] B. Zhao, X. Zhang, J. Chen, C. Wang, and L. Guo, "Operation optimization of standalone microgrids considering lifetime characteristics of battery energy storage system," *IEEE Trans. Sustain. Energy*, vol. 4, no. 4, pp. 934–943, Oct. 2013.

[122] L. Wang and C. Singh, "Multicriteria design of hybrid power generation systems based on a modified particle swarm optimization algorithm," *IEEE Trans. Energy Convers.*, vol. 24, no. 1, pp. 163–172, Mar. 2009.

[123] S. Sinha and S. Chandel, "Review of recent trends in optimization techniques for solar photovoltaic-wind based hybrid energy systems," *Renewable Sustain. Energy Rev.*, vol. 50, pp. 755–769, 2015.

[124] H. Yang, W. Zhou, L. Lu, and Z. Fang, "Optimal sizing method for stand-alone hybrid solar-wind system with LPSP technology by using genetic algorithm," *Sol. Energy*, vol. 82, no. 4, pp. 354–367, 2008.

[125] B. Ould Bilal, V. Sambou, P. Ndiaye, C. Kébé, and M. Ndongo, "Optimal design of a hybrid solar-wind-battery system using the minimization of the annualized cost system and the minimization of the loss of power supply probability (LPSP)," *Renewable Energy*, vol. 35, no. 10, pp. 2388–2390, 2010.

[126] Y. Cheng, M. Chuang, Y. Liu, S. Wang, and Z. Yang, "A particle swarm optimization based power dispatch algorithm with roulette wheel re-distribution mechanism for equality constraint," *Renewable Energy*, vol. 88, pp. 58–72, 2016.

[127] P. Paliwal, N. Patidar, and R. Nema, "Determination of reliability constrained optimal resource mix for an autonomous hybrid power system using particle swarm optimization," *Renewable Energy*, vol. 63, pp. 194–204, 2014.

[128] H. Borhanazad, S. Mekhilef, V. Gounder Ganapathy, M. Modiri-Delshad, and A. Mirtaheri, "Optimization of micro-grid system using MOPSO," *Renewable Energy*, vol. 71, pp. 295–306, 2014.
[129] A. R. Prasad and E. Natarajan, "Optimization of integrated photovoltaic-wind power generation systems with battery storage," *Energy*, vol. 31, no. 12, pp. 1943–1954, 2006.
[130] U. Boonbumroong, N. Pratinthong, S. Thepa, C. Jivacate, and W. Pridasawas, "Particle swarm optimization for AC-coupling stand alone hybrid power systems," *Sol. Energy*, vol. 85, no. 3, pp. 560–569, 2011.
[131] B. Y. Ekren and O. Ekren, "Simulation based size optimization of a PV/Wind hybrid energy conversion system with battery storage under various load and auxiliary energy conditions," *Appl. Energy*, vol. 86, no. 9, pp. 1387–1394, 2009.
[132] H. Yang, Z. Wei, and L. Chengzhi, "Optimal design and techno-economic analysis of a hybrid solar-wind power generation system," *Appl. Energy*, vol. 86, no. 2, pp. 163–169, 2009.
[133] D. P. Clarke, Y. M. Al-Abdeli, and G. Kothapalli, "Multi-objective optimisation of renewable hybrid energy systems with desalination," *Energy*, vol. 88, pp. 457–468, 2015.
[134] M. B. Shadmand and R. S. Balog, "Multi-objective optimization and design of photovoltaic-wind hybrid system for community smart DC microgrid," *IEEE Trans. Smart Grid*, vol. 5, no. 5, pp. 2635–2643, Sep. 2014.
[135] F. Giraud and Z. M. Salameh, "Steady-state performance of a grid-connected rooftop hybrid wind-photovoltaic power system with battery storage," *IEEE Trans. Energy Convers.*, vol. 16, no. 1, pp. 1–7, Mar. 2001.
[136] R. Hosseinalizadeh, H. Shakouri G, M. S. Amalnick, and P. Taghipour, "Economic sizing of a hybrid (PV-WT-FC) renewable energy system (HRES) for stand-alone usages by an optimization-simulation model: Case study of Iran," *Renewable Sustain. Energy Rev.*, vol. 54, pp. 139–150, 2016.
[137] A. Kaabeche, M. Belhamel, and R. Ibtiouen, "Sizing optimization of grid-independent hybrid photovoltaic/wind power generation system," *Energy*, vol. 36, no. 2, pp. 1214–1222, 2011.
[138] A. Hassan, M. Kandil, M. Saadawi, and M. Saeed, "Modified particle swarm optimisation technique for optimal design of small renewable energy system supplying a specific load at mansoura university," *IET Renewable Power Gener.*, vol. 9, no. 5, pp. 474–483, 2015.
[139] A. Maleki, M. Ameri, and F. Keynia, "Scrutiny of multifarious particle swarm optimization for finding the optimal size of a PV/Wind/Battery hybrid system," *Renewable Energy*, vol. 80, pp. 552–563, 2015.
[140] H. Baghaee, M. Mirsalim, G. Gharehpetian, and H. Talebi, "Reliability/cost-based multi-objective Pareto optimal design of stand-alone Wind/PV/FC generation microgrid system," *Energy*, vol. 115, pp. 1022–1041, 2016.
[141] A. Askarzadeh and L. dos Santos Coelho, "A novel framework for optimization of a grid independent hybrid renewable energy system: A case study of Iran," *Sol. Energy*, vol. 112, pp. 383–396, 2015.
[142] B. Zhao, X. Zhang, P. Li, K. Wang, M. Xue, and C. Wang, "Optimal sizing, operating strategy and operational experience of a stand-alone microgrid on Dongfushan island," *Appl. Energy*, vol. 113, pp. 1656–1666, 2014.
[143] A. Ogunjuyigbe, T. Ayodele, and O. Akinola, "Optimal allocation and sizing of PV/wind/split-diesel/battery hybrid energy system for minimizing life cycle cost, carbon emission and dump energy of remote residential building," *Appl. Energy*, vol. 171, pp. 153–171, 2016.
[144] J. Zeng, M. Li, J. F. Liu, J. Wu, and H. W. Ngan, "Operational optimization of a stand-alone hybrid renewable energy generation system based on an improved genetic algorithm," in *Proc. IEEE PES Gen. Meeting*, 2010, pp. 1–6.
[145] A. Maleki and A. Askarzadeh, "Artificial bee swarm optimization for optimum sizing of a stand-alone PV/WT/FC hybrid system considering LPSP concept," *Sol. Energy*, vol. 107, pp. 227–235, 2014.
[146] S. Tito, T. Lie, and T. Anderson, "Optimal sizing of a wind-photovoltaic-battery hybrid renewable energy system considering socio-demographic factors," *Sol. Energy*, vol. 136, pp. 525–532, 2016.
[147] P. Roy, J. He, and Y. Liao, "Cost minimization of battery-supercapacitor hybrid energy storage for hourly dispatching wind-solar hybrid power system," *IEEE Access*, vol. 8, pp. 210099–210115, 2020.

PRANOY ROY (Graduate Student Member, IEEE) received the B.Sc. degree in electrical and electronics engineering from the Rajshahi University of Engineering & Technology, Rajshahi, Bangladesh, and the M.Sc. degree in engineering technology from Western Carolina University, Cullowhee, NC, USA. He is currently working toward the Ph.D. degree in electrical engineering with the University of Kentucky, Lexington, KY, USA, focusing on high-performance renewable energy and power electronic systems. To date, his research has yielded multiple peer-reviewed conference and journal papers.

JIANGBIAO HE (Senior Member, IEEE) received the Ph.D. degree in electrical engineering from Marquette University, Milwaukee, WI, USA. He is currently with the Department of Electrical and Computer Engineering, University of Kentucky, Lexington, KY, USA. He previously worked in industry, most recently as a Lead Engineer with GE Global Research, Niskayuna, NY, USA. Before he joined GE in 2015, he was also with Eaton Corporation and Rockwell Automation. He has authored and coauthored more than 110 technical papers and ten U.S. patents. His research interests include transportation electrifications (such as electric aircraft and vehicles), renewable energies, and fault-tolerant electric power apparatuses for safety-critical applications.

Dr. He was the Editor or an Associate Editor for several prestigious journals in electric power area. He also served in various roles in the organizing committees for numerous IEEE international conferences, and has been an active member of multiple IEEE standards working groups. He was the recipient of the 2019 AWS Outstanding Young Member Achievement Award recognized by the IEEE Industry Applications Society.

TIEFU ZHAO (Senior Member, IEEE) received the B.S. and M.S. degrees from Tsinghua University, Beijing, China, in 2003 and 2005, respectively, and the Ph.D. degree from North Carolina State University, Raleigh, NC, USA, in 2010, all in electrical engineering.

From 2010 to 2016, he was with Eaton Corporation Research and Technology, Milwaukee, WI, USA. Since 2016, he has been an Assistant Professor of electrical and computer engineering and an Associate with the Energy Production and Infrastructure Center (EPIC), University of North Carolina, Charlotte, NC, USA. He has authored or coauthored more than 40 papers in refereed journals and international conference proceedings. He has 12 patents awarded. His current research interests include solid state transformer, solid state circuit protection, wireless power transfer, wide bandgap device-based power conversion, power electronics reliability, and fault detection.

Dr. Zhao was an Associate Editor for the IEEE JOURNAL OF EMERGING AND SELECTED TOPICS IN POWER ELECTRONICS.

YASH VEER SINGH (Member, IEEE) received the M.Tech. degree in electrical engineering from the Indian Institute of Technology Bombay, Mumbai, India, in 2007, and the Ph.D. degree from Aalborg University, Aalborg, Denmark in 2016, while working on an industrial sponsored program by Danfoss drive during 2008–2011. Since May 2021, he has been a Technology Manager of power electronics with Eaton Research Lab (ERL), Southfield, MI, USA. In June 2019, he joined ERL, as a Senior Specialist Power Conversion in Menomonee Falls, WI, USA. He was with GE Global Research in Bangalore, India, between December 2011 and June 2016 and in Niskayuna, NY, USA, from June 2016 to June 2019. His work with GE was on power conversion for aviation and healthcare applications, including CT and MRI scanners. He has more than ten publications in IEEE and other conferences and more than 13 U.S. patents issued or filed. His research interests include high density power conversion for transportation and design of power converters with soft switching features, designing, developing and testing power electronics platforms and systems for power conversion and distribution applications.